



## 1 **The 2024 cascading glacial lake outburst flood in the Thame Valley** 2 **of Everest region, Nepal: process, impacts and implications**

3 Nitesh Khadka<sup>1</sup>, Vishnu Prasad Pandey<sup>1, 2 \*</sup>, C. Scott Watson<sup>3</sup>, Guoxiong Zheng<sup>4, 5</sup>, Tianpei Wu<sup>6, 7</sup>,  
4 Keshab Sharma<sup>8</sup>, Lauren D. Rawlins<sup>3</sup>, Simon Allen<sup>9</sup>, Manish Raj Gouli<sup>10</sup>, Dibas Shrestha<sup>11</sup>

5 <sup>1</sup>Center for Water Resources Studies (CWRS), Institute of Engineering, Tribhuvan University, Lalitpur, Nepal

6 <sup>2</sup>Department of Civil Engineering, Pulchowk Campus, Institute of Engineering, Tribhuvan University, Lalitpur, Nepal

7 <sup>3</sup>School of Geography and water@leeds, University of Leeds, Leeds, UK

8 <sup>4</sup>College of Earth and Environmental Sciences, Lanzhou University, Lanzhou, China

9 <sup>5</sup>Midui Glacier-Guangxie Lake Disaster Field Science Observation and Research Station of Tibet Autonomous Region,  
10 Northwest Institute of Eco-Environment and Resources, Chinese Academy of Sciences, Lanzhou, China

11 <sup>6</sup>State Key Laboratory of Mountain Hazards and Engineering Resilience, Institute of Mountain Hazards and  
12 Environment, Chinese Academy of Sciences, Chengdu, China

13 <sup>7</sup>University of Chinese Academy of Sciences, Beijing, China

14 <sup>8</sup>BGC Engineering Inc., 330 Alison Blvd., Fredericton, NB, Canada E3C 0A9

15 <sup>9</sup>Department of Geography, University of Zurich, Zurich, Switzerland

16 <sup>10</sup>The Stimson Center - Energy, Water, & Sustainability, 1211 Connecticut Ave, NW / 8th Floor Washington, DC 20036

17 <sup>11</sup>Central Department of Meteorology and Hydrology, Tribhuvan University, Kathmandu, Nepal

18

19 **\*Correspondence:** Vishnu Prasad Pandey ([vishnu.pandey@pcampus.edu.np](mailto:vishnu.pandey@pcampus.edu.np))

20 **Abstract.** On the afternoon of 16 August 2024, a catastrophic flood devastated Thame Village in the Everest region of  
21 Nepal. This event resulted from a cascading glacial lake outburst flood (GLOF), where the outburst of an upstream  
22 glacial lake triggered the failure of a downstream lake in the headwaters—a complex hazard chain often-overlooked in  
23 conventional risk assessments. By integrating multi-source satellite imagery, field data, climatic data, empirical  
24 estimations, and numerical modelling, we analyse the triggers, processes, and consequences of the cascading failure. We  
25 find that the upper lake, which formed in the late 2000s, expanded rapidly to 0.11 km<sup>2</sup> prior to its outburst, while the  
26 lower lake grew by 20% between 1989 and 2024. The hydrological tipping point for the upper lake was driven by intense  
27 glacier melt and calving from extreme temperatures and precipitation. Its overtopping triggered a cascade, causing the  
28 breach of the lower lake's moraine dam and releasing a combined water volume of approximately  $6 (\pm 0.65) \times 10^5$  m<sup>3</sup>.  
29 Multi-phase mass flow modelling reconstructing two possible scenarios indicates that the flood wave, with an initial peak  
30 discharge exceeding 800 m<sup>3</sup>/s, reached Thame Village within 22 to 32 minutes. The socio-economic impact was severe,  
31 with losses estimated at 6.18 million USD within the Khumbu Pasang Lhamu Rural Municipality alone, and flood effects  
32 traced over 50 km downstream. This event demonstrates that small, rapidly evolving glacial lakes, conditioned by  
33 climate-induced glacier retreat, can generate devastatingly powerful GLOFs. This underscores a critical need to broaden  
34 GLOF risk assessments to include such small lakes and to prioritize reducing exposure and vulnerability in dynamic  
35 high-mountain communities over solely engineering-based hazard control.

36

37 **Keywords:** cascading GLOF, climate change, disaster risk reduction, multi-phase mass flow, Thame Valley



## 38 1 Introduction

39 Glacial Lake Outburst Floods (GLOFs) are high-magnitude events in mountainous regions that can evolve into hyper-  
40 concentrated or debris flows, leading to substantial hydrological, geomorphological, and socio-economic impacts  
41 downstream (Cook et al., 2018; Veh et al., 2020; Sattar et al., 2025). A total of 569 reported GLOF events have been  
42 documented over High Mountain Asia (HMA) till 2022 (Lützwow et al., 2023). Across HMA, the risk of GLOF is  
43 expected to increase in future by three-fold amidst ongoing climate change induced glacial recession and evolution of  
44 glacial lakes (Zheng et al., 2021b). Thus, risk assessment of present glacial lakes (Zhang et al., 2023c) and modelling  
45 future lake formation and predicting their GLOF hazard (Furian et al., 2021; Zheng et al., 2021b; Furian and Sauter,  
46 2025) are essential works for the early identification of GLOF risk hotspots. Current regional scale (Allen et al., 2019;  
47 Zhang et al., 2022), national scale (Rounce et al., 2017; Dubey and Goyal, 2020; Chen et al., 2025) to case specific  
48 GLOF risk assessments and field studies (Sattar et al., 2021; Allen et al., 2022; Rinzin et al., 2023; Gouli et al., 2025) in  
49 the Himalayan region are mainly targeted at glacial lakes of considerable size, often neglecting small glacial lakes owing  
50 to their low potential flood volume. However, global assessment shows the dominance of outburst floods from small  
51 glacial lakes (Veh et al., 2025). Additionally, GLOF events in the Himalaya such as 2013 Kedarnath disaster in India  
52 (Allen et al., 2016), 2016 Gonbatongshaco GLOF in China-Nepal border (Sattar et al., 2022; Chen et al., 2023) and 2017  
53 Langmale GLOF (Byers et al., 2018) have shown that GLOFs from small lakes can also cause devastation downstream.

54 On 16<sup>th</sup> August of 2024 at 1.30 pm, Thame Village in the Everest region of Nepal experienced a massive flooding,  
55 prompting authorities to issue alerts for the downstream region. The following day, a helicopter survey by Government  
56 of Nepal revealed that this flooding was triggered by a cascading outburst of two glacial lakes located in the headwaters  
57 of Thame Valley (Ghimire, 2024). These lakes were relatively small in size ( $<0.1 \text{ km}^2$ ) compared to nearby glacial lakes  
58 such as Tsho Rolpa ( $1.67 \text{ km}^2$  in 2022) and Imja Tsho ( $1.73 \text{ km}^2$  in 2022) which have been studied in detailed (Icimod,  
59 2011; Khadka et al., 2019) and also have undergone GLOF remediation works (Cuellar and Mckinney, 2017; Lala et al.,  
60 2018). Due to their relatively small size, these lakes were missed in the previous GLOF hazard and risk assessments at  
61 regional and local scales (Table 1). Among previous studies, Zhang et al. (2023c) included these glacial lakes in their  
62 comprehensive GLOF risk assessments in HMA and reported one lake (upper lake 1, Fig. 1) to have high GLOF hazard.  
63 Site-specific investigation of GLOFs and dissemination of information, including their occurrence dates, triggers, process  
64 and impacts, is essential for understanding of the nature and behaviour of outburst floods, particularly in the context of  
65 climate change (Westoby et al., 2014; Mergili et al., 2018a; Nie et al., 2020). Several studies have studied the evolution,  
66 triggers and reconstructed the past GLOF events. For example, 2001 Chongbaxiaco GLOF in eastern Himalaya (Nie et  
67 al., 2020), 2014 Gya GLOF in Indian Himalaya (Majeed et al., 2021), 2018 Langmale GLOF at Nepal (Byers et al.,  
68 2018), 2002 and 2016 GLOFs in Poiqu river basin, central Himalaya (Wang et al., 2024), 2020 Jinwucuo GLOF in Tibet  
69 (Zheng et al., 2021a), 2023 South Lhonak GLOF (Sattar et al., 2025; Zhang et al., 2025) and 2024 Birendra lake GLOF  
70 (Khadka et al., 2024b; Poudel et al., 2025) were analysed and reconstructed. These studies collectively not only provide  
71 insights into mechanisms and triggers of GLOFs but also contribute to enhance the future GLOF risk assessment  
72 frameworks, better develop GLOF models, and finally aid in effective disaster risk reduction and mitigation strategies.

73 The outburst of lower Ngole glacial lake was due to an outburst from the upper glacial lake. When multiple lakes are  
74 arranged in series within a watershed, the overtopping or failure of an upstream lake may trigger a cascading breach of  
75 downstream lakes, generating a “domino effect” that substantially amplifies flood magnitude and destructive potential  
76 through flow bulking. This GLOF occurred during the monsoon season (June to September), a period characterized by



77 elevated temperatures, significant precipitation, and increased river discharge (Salerno et al., 2015; Sharma et al., 2020).  
 78 The cascading GLOF resulted in severe damage to Thame Village, trekking trails and several infrastructures in the  
 79 Everest region. In this study, we aim to (i) track the long-term evolution of these two glacial lakes using satellite  
 80 observations, (ii) identify the possible triggers, (iii) analyse the conditioning factors that led to the trigger, (iv) reconstruct  
 81 the cascading GLOF process chain using numerical modelling, and (v) report the downstream impacts of the GLOF.  
 82 Further, we assess and discuss the potential future GLOF hazard from these lakes and outline several strategies for GLOF  
 83 risk reduction in the area. Finally, this study will contribute to better understanding of the cascading Thame GLOF  
 84 process chain and underscores the need to reconsider the prioritization of small glacial lakes in future GLOF risk  
 85 assessment and disaster risk management in the high Himalayan regions.

86

87 **Table 1. List of studies that have identified dangerous glacial lakes including the Everest region of Nepal.**

Study	Study area	Method	Minimum lake size (km <sup>2</sup> )
Icimod (2011)	Nepal	Qualitative	>0.2
Rounce et al. (2017)	Nepal	Quantitative and decision-based classification	≥0.1
Bajracharya et al. (2020)	Nepal and transboundary areas	Qualitative	≥0.2
Khadka et al. (2021)	Mahalangur Himal	Quantitative: Weight based multi-criteria	≥0.05
Zheng et al. (2021b)	HMA	Quantitative with equal weights	≥0.05
Hu et al. (2022)	Nepal	Quantitative: Weight based multi-criteria	≥0.2
Zhang et al. (2023c)	HMA	Quantitative: Weight based multi-criteria	≥0.01

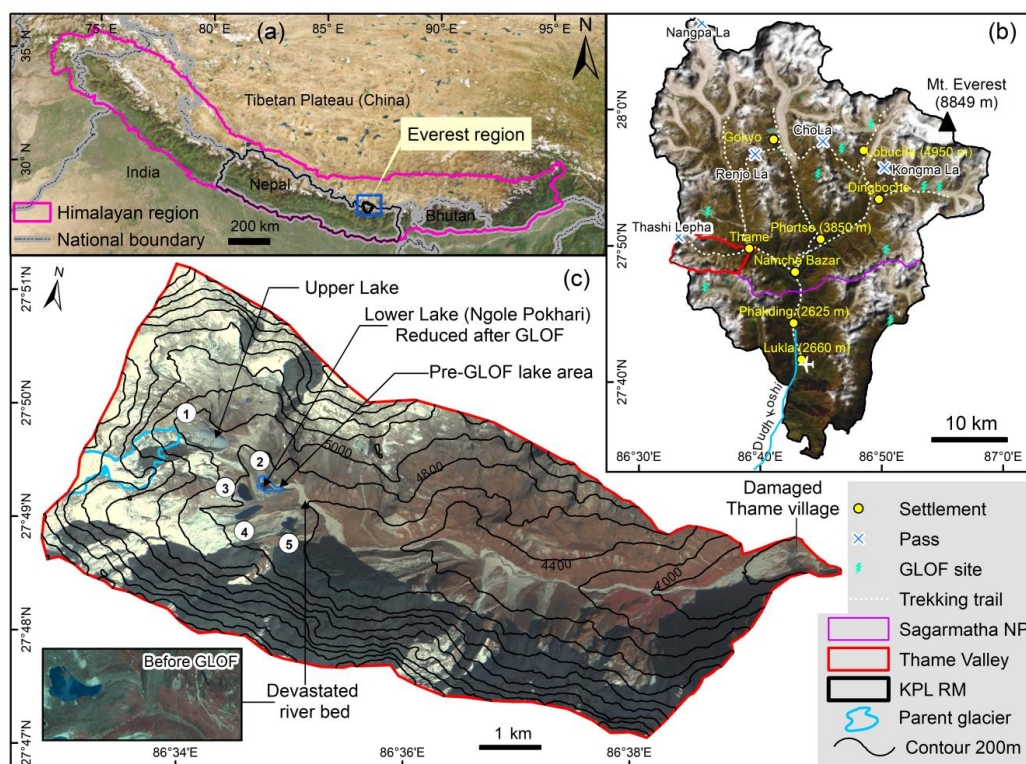
## 88 2 Study area

89 The present GLOF site is located in the Thame Valley of DudhKoshi basin of eastern Nepal Himalaya, often also  
 90 referred as Everest region or Khumbu Himal (Figure 1) (Byers, 2017). Nepal Himalaya hosts dense distribution of  
 91 glaciers and glacial lakes in the northern part of country (Khadka et al., 2023). In response to climatic warming, glaciers  
 92 in Nepal have shrunk by 14% between 1970 and 2010 (Khadka et al., 2023) whereas the surface area of glacial lakes  
 93 have undergone 25% expansion between 1987 and 2017 (Khadka et al., 2018). The climate of this region is affected by  
 94 South Asian monsoon in summer and by westerlies in winter (Salerno et al., 2015). Most glaciers in the Everest region  
 95 are valley type with debris covered in the ablation zone (Thakuri et al., 2014). Nine large glaciers in the region exhibited  
 96 negative mass balance of  $-0.52 \pm 0.22$  m water equivalent (w.e.) a<sup>-1</sup> during 2000–2015 (King et al., 2017). Among  
 97 different regions of Nepal, the expansion rate of glacial lakes is reported to be highest (1.37 km<sup>2</sup> per decade) in the  
 98 Everest region (Khadka et al., 2018). Everest region has witnessed at least nine GLOF events (Figure 1b), among which  
 99 1985 Dig Tsho GLOF (Vuichard and Zimmermann, 1987) and 1998 Tam Pokhari GLOF (Lamsal et al., 2016) caused  
 100 notable downstream socio-economic impacts.

101 The Thame Valley lies in the east of Sagarmatha National Park under Khumbu Pashung Lamu Rural Municipality (KPL  
 102 RM) Ward Number 5, which had a population of 1255 in 2021 (National Statistic Office, 2023). Thame Village at an  
 103 elevation of 3,800 m a.s.l (above sea level) is 5 km from Namche bazar, a touristic town and gateway to Mt. Everest.  
 104 Thame Village enroute to Thashi Lepcha pass and Renjo La pass attracts many tourists, has a small hydroelectric power  
 105 plant (930 kW), numerous houses, lodges and restaurants, Buddhist Monastery, health post and a school. The headwaters



106 of the valley are home to seven glacial lakes, five of which are clustered in close proximity to one another (Fig. 1c). The  
 107 upper glacial lake 1 (4,890 m a.s.l) experienced a breach that triggered an outburst from the lower glacial lake, known as  
 108 Ngole Pokhari (where “Pokhari” meaning “pond” in Nepali), leading to a cascading GLOF. The upper lake is situated at  
 109 the terminus of a debris-covered glacier (G086552E27827N) with a catchment area of ~5 km<sup>2</sup>, and is dammed by  
 110 bedrock, overlaid with glacial moraine. The lower glacial lake 2 (4,718 m a.s.l) is a moraine-dammed lake with a  
 111 catchment area of ~9 km<sup>2</sup>, located approximately 700 m below the upper lake and is part of the same glacier that has  
 112 retreated since the end of the Little Ice Age and now no longer exists (Fig. S1) (Lee et al., 2021). The moraine dam of  
 113 lower lake is composed of a diverse and well-graded mixture of silt, sand, gravel, cobbles, and boulders, with some clast  
 114 sizes reaching or even exceeding 5 m in diameter (Figure 2).



115  
 116 **Figure 1: Study area showing the location of GLOF site. Study area in the border regional level (a) and at Khumbu Pasang**  
 117 **Lamu Rural Municipality (KPL RM) of Nepal (b) with enlarged Thame Valley showing the topography after the GLOF event**  
 118 **(c). The base images (a and b) are produced by ESRI (Sources: Esri, TomTom, FAO, USGS | Powered by Esri) and a Gaofen**  
 119 **image of August 18, 2024 (c). The figure was created by authors using ArcGIS® software by Esri.**

### 120 3 Materials and Methods

121 We employed a variety of data sources for this study, including multi-source optical remote sensing data, digital  
 122 elevation models (DEM), reanalysis and station-based climate data, field measurements, and additional auxiliary  
 123 datasets. A summary of these datasets is presented in Table 2, while the subsequent sections detail their specific  
 124 applications in the study.



125

126 **Table 2. Datasets used in this study for various purposes.**

No.	Data	Acquisition date	Repeat cycle (days)	Spatial resolution (m)	Purpose
1	Landsat MSS*	1976-11-13	16	60	Lake mapping
2	Landsat-5 TM*	1989-11-09; 1995-10-09; 2000-11-23; 2010-12-05	16	30	Lake mapping
3	Landsat-8 OLI*	2015-11-17	16	30	Lake mapping
4	Sentinel-2	2020-10-09; 2022-05-17; 2024-11-27; 2025-03-29	5	10	Lake mapping
5	Planet Scope	2024-08-15; 2024-08-16	1	3	Lake mapping, and cause analysis of GLOF
6	Gaofen-2/7	2024-05-30; 2024-08-18; 2024-10-31	Gaofen-2: 16 Gaofen-7: 12	1-0.65	Lake mapping, cause and impact analysis of GLOF
7	HMA-DEM	2014-2016 mosaic (MO_20170716_tile-677)	-	8	Topographic analysis and GLOF process chain
8	ERA5 Land (reanalysis data)	1990-2024	hourly	9 km	Climatological study and cause analysis
9	Meteorological station data	2019-2024	hourly	daily	Climatological study (support to reanalysis data)
10	Composite Ice thickness (raster data)	2020	-	-	To know the tentative height of icebergs

127 \*MSS- Multi-spectral Scanner; TM-Thematic Mapper; OLI-Operational Land Imager

128 **3.1 Delineation of glaciers and glacial lakes**

129 We used multi-source optical remote sensing datasets (Table 2) to track the area of glacier and glacial lakes from 1976 to  
 130 2024. Glacier and glacial lake outlines were manually delineated from the geometrically corrected false colour composite  
 131 images (NIR/red/green) of satellite data by a single expert (Wang et al., 2020). The error associated with the delineation  
 132 of individual lake boundaries was calculated as the product of half the image resolution and the lake’s perimeter. This  
 133 error calculation is predicted on the assumption that, on average, the lake margin intersects the centres of the pixels along  
 134 its perimeter (Salerno et al., 2012).

135 **3.2 Field-based and empirical quantification of the event and cause analysis**

136 During field investigation (Nov-Dec 2024), we engaged with local residents of Thame Village, stakeholders and rural  
 137 municipality to gather insights on the timing and impacts of this event. We explored the potential causes of this GLOF  
 138 and employed a Global Positioning System (GPS) to measure the lowering of the lake levels after their outbursts. We  
 139 utilized a laser range finder to assess the width and depth of the breach in the moraine dam of the glacial lakes (Figure 2),  
 140 changes in river morphology, and geomorphology in Thame Village. Additionally, the breach parameters were obtained  
 141 and verified from the field report of International Centre for Integrated Mountain Development (ICIMOD) (Maharjan et  
 142 al., 2025).

143 A post-GLOF bathymetric survey of the lower lake was conducted in May 2025 using an uncrewed surface vessel  
 144 (USV). Concurrently, a high-resolution (1 m) DEM was acquired via uncrewed aerial vehicle (UAV) surveys. The  
 145 drainage volume from the lower lake was reconstructed by integrating the pre-GLOF lake volume derived from the DEM  
 146 with the post-GLOF lake volume derived from bathymetry (details in supplementary Text S1). The bathymetric



147 measurements could not be obtained for the upper lake due to surface ice cover, which prevented a survey. To ensure  
 148 methodological consistency across both lakes, we therefore relied on empirical volume–area equations to estimate the  
 149 drained volumes for both the upper and lower lakes. Notably, the reconstructed drainage volume for the lower lake shows  
 150 close agreement with the empirical estimates, thereby supporting the reliability of the empirical approach (Text S1).  
 151 Thus, the volumes of water in the lake before and after the GLOF were empirically estimated using nine area-volume  
 152 relationships (see Tables 3 and S1). For this, lake area estimated before (2024-08-15) and after (2024-08-18) the event  
 153 was utilized. The difference in volume between the pre-GLOF and post-GLOF measurements was regarded as the  
 154 drained volume. The average of all nine estimations was then calculated to determine the overall released volume (Table  
 155 S1). The standard deviation of the drained volume for each lake was adopted as the volumetric uncertainty. The total  
 156 uncertainty associated with the cascading GLOF was then computed as the root-sum-square of the individual  
 157 uncertainties from the upper and lower lakes.

158 The peak discharge during the GLOF event and the timing of the dam breach formation were also derived empirically  
 159 based on the released volume and lake lowering height. The released volume was calculated as described above, while  
 160 the lake lowering height and breach dimensions were determined through field measurements (Figure 2). Various  
 161 empirical equations commonly found in the literature were utilized for estimation purposes, and the overall average of  
 162 these calculations was taken as the final estimate for both peak discharge and the timing of breach formation (Tables 3  
 163 and S2). The total volume released, peak discharge, and timing of the dam breach for the cascading event were analysed  
 164 by combining the released volumes from both the upper and lower lakes (Tables S1 and S2).

165 The different possible triggering factors of the GLOF were analysed based on field observations, published news/reports  
 166 and through examination of fine-resolution remote sensing images (See Section 4.2). Icebergs were manually delineated  
 167 from PlanetScope (3 m) and Gaofen-7 images (0.65 m) of 2024-8-15/16 and 2024-08-18, respectively. The icebergs, both  
 168 pre- and post-GLOF, as well as those that are grounded and drifting, were identified through a comparative analysis of  
 169 the images (Fig. S2). The volume of icebergs was determined based on the area-volume relationship as shown in  
 170 Equation 1. This equation was derived by Watson et al. (2020) through detailed study of calving and iceberg formation of  
 171 Thulagi glacial lake in Nepal.

172  
 173 
$$V_i = 4.3017A^{1.19} \dots \dots \dots \quad (1)$$

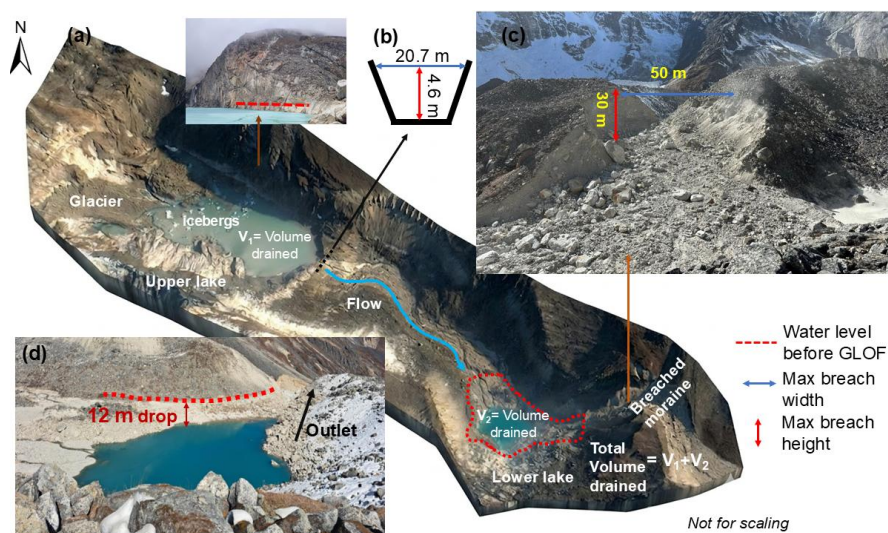
174 Where,  $V_i$  is volume of icebergs in  $m^3$  and  $A$  is surface area of icebergs in  $m^2$ .

175  
 176

177 **Table 3. Studies whose empirical equations were used to calculate three parameters. The details of the equations and the**  
 178 **calculations are given in supplementary Tables S1 and S2.**

Parameter calculated	Studies whose empirical equations were used
Lake Volume (V)	Evans (1986); Huggel et al. (2002); Wang et al. (2012); Sakai (2012); Khanal et al. (2015); Cook and Quincey (2015); Kapitsa et al. (2017); Zhang et al. (2023a); Zhang et al. (2023b)
Peak discharge	Evans (1986); Popov (1991); Costa and Schuster (1988); Costa (1985); Costa (1985); Froehlich (1995); Froehlich (2025)
Breach time	Froehlich (1995); Froehlich (2025)

179



180

181 **Figure 2: Images showing the breach mechanism and associated breach parameters following the cascading GLOF. (a) The**  
 182 **outburst of upper lake cascades into lower lake, resulting its outburst, which is characterized by a reduced water level and a**  
 183 **breached terminal moraine. (b) Breach parameters of the upper lake and (c) lower lake and (d) observed decrease in water**  
 184 **level of the lower lake. The image in (a) is from Gaofen-7 satellite while those in (c) and (d) are obtained from field.**

### 185 3.3 Climatic analysis

186 We used ERA-5 Land data, the global reanalysis dataset which provides long-term data on climate variables since 1950  
 187 (Muñoz-Sabater et al., 2021) and has good performance in the Nepal Himalaya (Chen et al., 2021). ERA5-Land dataset  
 188 aggregated at daily timestep was accessed using the Google Earth Engine (GEE) platform. Daily aggregates in GEE are  
 189 pre-calculated daily from hourly values. We extracted the daily aggregated 2-m air temperature (24-hour average) and  
 190 precipitation (24-hour total) for the lake area from 1990 to 2024. The days with extreme temperature and precipitation  
 191 exceeding 90<sup>th</sup> and 95<sup>th</sup> percentiles were calculated with respect to long-term time series (1990–2024) data. Additionally,  
 192 data from the Phortse Automatic Weather Station, located 11 km east of Thame Village at the same elevation (3,850 m),  
 193 was utilized to obtain observed values of temperature and precipitation for the area.

### 194 3.4 Cascading GLOF simulation with r.avafLOW

195 Cascading GLOF processes were simulated using r.avafLOW (v. 4.0G), an open-source multi-phase computational tool for  
 196 complex mass flow dynamics in mountain regions (Mergili and Pudasaini, 2014-2025). Unlike traditional single-phase  
 197 models, r.avafLOW employs a coupled multi-phase approach to accurately characterize phase interactions and material  
 198 entrainment, enhancing the simulation of cascading hazards (Mergili et al., 2017). Its core algorithm, developed by  
 199 Pudasaini and Mergili (2019), propagates mass flow across a DEM using depth-averaged continuity and momentum  
 200 equations (Mergili et al., 2018b). The model employs a second-order TVD-NOC (Total Variation Diminishing Non-  
 201 Oscillatory Central Differencing) scheme on a staggered grid for spatial discretization, ensuring both accuracy and  
 202 stability (Tai et al., 2002). Operating with GIS raster cells, it facilitates mass-flow exchanges between adjacent cells at  
 203 each time step (Mergili et al., 2025). Integrated within GRASS GIS 7, r.avafLOW combines Python/C code with R-based  
 204 statistical tools for efficient simulation and analysis, as detailed by Mergili et al. (2017). The model’s capabilities include  
 205 the consideration of rock, ice, and fluid phases, and incorporates a multi-phase thermo-mechanical model that features



206 equations for the transition from ice to liquid, which is primarily influenced by heat from inter-phase friction. This  
207 framework allows for the investigation of cascading hazards in cold, high-altitude regions, including ice-rock avalanches,  
208 landslides, debris flows, and floods.

209 We modelled the cascading GLOF process chain based on two scenarios that encapsulate the extremes of potential  
210 mechanisms within the event. In Scenario A, we assumed a rapid inflow generated by the upstream lake breach entered  
211 the downstream lake and produced displacement wave that overtopped the dam crest and progressively eroded the  
212 moraine dam. However, in Scenario B, the inflow from the upstream lake was assumed that gradually increased the water  
213 level (and storage volume) of the downstream lake until it reached the dam crest, subsequently resulting in dam failure.

214 For GLOF simulation, the volume of the lake, peak discharge, and breach timing were empirically estimated (Sections  
215 3.2 and 4.2), while other dam and breach parameters were sourced from field measurements (Figure 2). For both  
216 scenarios, lower lake volume modelling was performed using `r.lakefill` function within `r.avaflow`, which is primarily  
217 analysed based on GRASS GIS. Following previous moraine dam GLOF studies, the value of the lake dam entrainment  
218 coefficient was taken as  $10^{-5.7}$  (Zhang et al., 2025). In Scenario A, an idealized triangular hydrograph (Huggel et al.,  
219 2002; Froehlich, 2025) was developed based on upper lake empirical estimates of volume and peak discharge for input  
220 into the lower lake (see Fig. S3). For Scenario B, a GIS-based analysis was conducted, revealing that the drained  
221 upstream lake volume resulted in 11.8 m rise in water level prior that exceeded the dam crest leading to the dam's failure.

222 Other essential input parameters for the simulations in both scenarios are summarized in Table 4 which were mainly  
223 derived from existing studies (Mergili et al., 2020b; Rinzin et al., 2025; Zhang et al., 2025; Chen et al., 2026) and  
224 obtained through optimization at the early stage of simulation. The HMA-DEM (Table 2) was utilized to represent the  
225 terrain owing to its greater resolution and all simulations were executed with a cell size of 10 m. The total simulation  
226 duration was set to 3,600 seconds (1 hr). The analysis was confined to Thame Village, which is approximately 9 km  
227 downstream from the lake source, as this area experienced the most significant damage. This limitation was necessitated  
228 by the unavailability of HMA-DEM data further downstream, as well as to reduce uncertainties associated with the  
229 complex topography of the Himalayan region.

230 The accuracy assessment of GLOF reconstruction was conducted by comparing the satellite-derived inundation area with  
231 the modelled flood extent. An overlay analysis was performed to calculate true positive, false positive, and false negative  
232 areas (see Text S2). From these, precision and recall were computed, followed by the F1 Score to provide a balanced  
233 measure of overall inundation accuracy (Text S2). These metrics yield a score between 0 and 1, with 1 indicating a  
234 perfect alignment between the two datasets being compared (Rawlins et al., 2026).

235

236 **Table 4 Basic input parameters used for `r.avaflow` simulation.**

Parameter	Unit	Value
Cell size	m	10
Density of solid phase ( $\rho_s$ )	kg/m <sup>3</sup>	2,700
Density of fluid phase ( $\rho_f$ )	kg/m <sup>3</sup>	1,000
Simulation time ( $T$ )	s	3,600
Internal friction angle ( $\Phi$ )	°	25
Basal friction angle ( $\delta$ )	°	15
Fluid friction number	-	0.05



237 **3.5 Impacts of the GLOF**

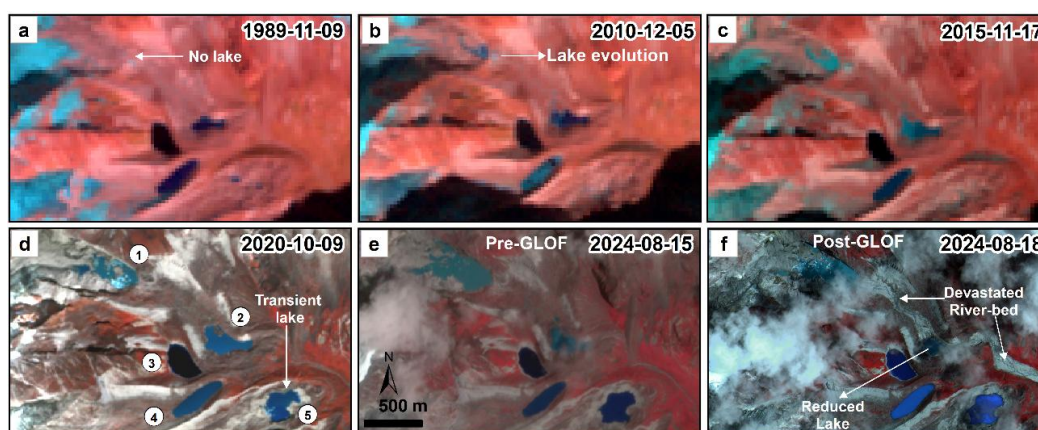
238 The impact assessment of the GLOF was conducted by synthesizing the detailed flood incident report on losses and  
239 damages compiled by the local government i.e., KPL RM (<https://khumbupasanglhamumun.gov.np/>). Furthermore,  
240 additional impacts were gathered from field study, news and intuitional reports and cross-verified using high-resolution  
241 images from the Gaofen-2/7.

242 **4 Results**

243 **4.1 Evolution of glacial lakes**

244 The evolution of the glacial lake cluster located in the headwaters of Thame Valley is shown in Fig. 3. The upper lake  
245 (Lake 1) started to form in the beginning of the 21<sup>st</sup> century with progression of its parent glacier shrinkage (Fig. 4a) and  
246 reached a considerable size of  $0.018 \pm 0.009 \text{ km}^2$  in 2010 (Figs. 3b and 4b). With rapid expansion in recent years (Fig.  
247 S4), it reached an area of  $0.11 \pm 0.004 \text{ km}^2$  before its outburst. After its outburst, the area slightly reduced by  $0.013 \text{ km}^2$ .

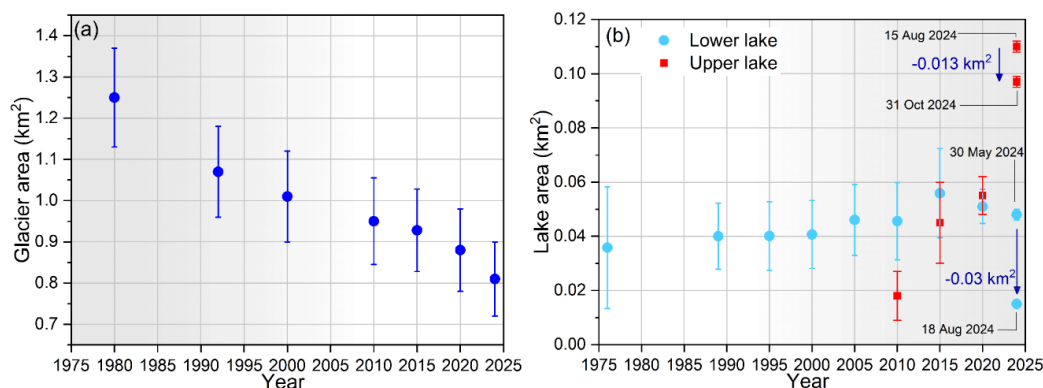
248 The lower lake (Lake 2) started to evolve before the 1980s, and it had an area of  $0.04 \pm 0.01 \text{ km}^2$  in 1989. It grew by 20%  
249 in the last 35 years (Fig. 4b). The area reduced from  $0.048 \pm 0.01 \text{ km}^2$  to  $0.015 \text{ km}^2$  after its outburst in August 16, 2024.  
250 The other lakes (lakes 3 and 4) on the southern sides were present from 1989 and a slight fluctuation of  $\pm 0.01 \text{ km}^2$  is  
251 observed between the years (Table S3). The Lake 5 is transient in nature and is mostly observed in monsoon season when  
252 snow-glacier melt and rainfall are common (Fig. S4). The areas of lakes 3, 4 and 5 are  $0.042$ ,  $0.042$  and  $0.01 \text{ km}^2$ ,  
253 respectively as derived from a Gaofen-7 image of 2024-08-18.



254

255 **Figure 3: The evolution of glacial lakes located in the headwaters of Thame Valley in the Everest region. The background**  
256 **images are from Landsat (a, b and c), PlanetScope (d and e) and Gaofen (f) satellites. The figure was created by authors using**  
257 **ArcGIS® software by Esri.**

258



259

260

Figure 4: Changes in the area of the parent glacier (a) and the upper and lower glacial lakes (b) from 1976 to 2024.

261

#### 4.2 Potential triggers and quantification of the event

262

Analysing the various potential triggering and conditioning factors (Table 5), it becomes evident that the likely cause for the outburst of the upper glacial lake is linked to extreme temperature-induced snow and glacier melt, coupled with calving from the parent glacier (debris-covered). These processes would increase the lake's water volume, which likely initiated a dam failure of the thin moraine dam, which overlaid bedrock (Figure 5).

266

The total surface areas of the delineated drifting icebergs ( $>130 \text{ m}^2$ ) in upper lake before the GLOF were  $3,117 \pm 1413 \text{ m}^2$  with corresponding volume of  $61,905 \pm 24,145 \text{ m}^3$  (Figure 5 and S2). We estimate icebergs to have a total height of  $\sim 15\text{-}25 \text{ m}$ , based on composite ice thickness raster data (Table 2) with more than 80 % to be considered submerged underwater. The glacier melting and calving events are linked to the extreme air temperatures (see Section 4.3). Our estimate indicates that approximately  $2.5 (\pm 0.3) \times 10^5 \text{ m}^3$  of water drained from the upper glacial lake. The lake level lowered by approximately 4.6 m and dam breached by approximately 21 m (Figure 2b). The total surface areas of the drifting ice-bergs ( $>20 \text{ m}^2$ ) after its outburst were  $7,092 \pm 1210 \text{ m}^2$  with a volume of  $162,921 \pm 19,982 \text{ m}^3$  (Figure 5d and S2).

274

The subsequent outburst flood from the upper glacial lake triggered the GLOF from lower glacial lake. The floodwaters from the upper lake descended approximately 172 m and travelled about 700 m before plunging into the lower lake (Fig. S1). The rapid influx of water and sediment substantially increased the volume of lower lake and generated surge waves in lake surface water that ultimately led to the failure of the moraine dam. Our estimate indicates that approximately  $3.5 (\pm 0.57) \times 10^5 \text{ m}^3$  of water drained from the lower glacial lake. Subsequently, the lake level has lowered by approximately 12 m and dam has incised by approximately 50 m (Figure 2).

280

A total of approximately  $6 (\pm 0.65) \times 10^5 \text{ m}^3$  of water was released from both lakes during the event.

281

282

283

284

285

286

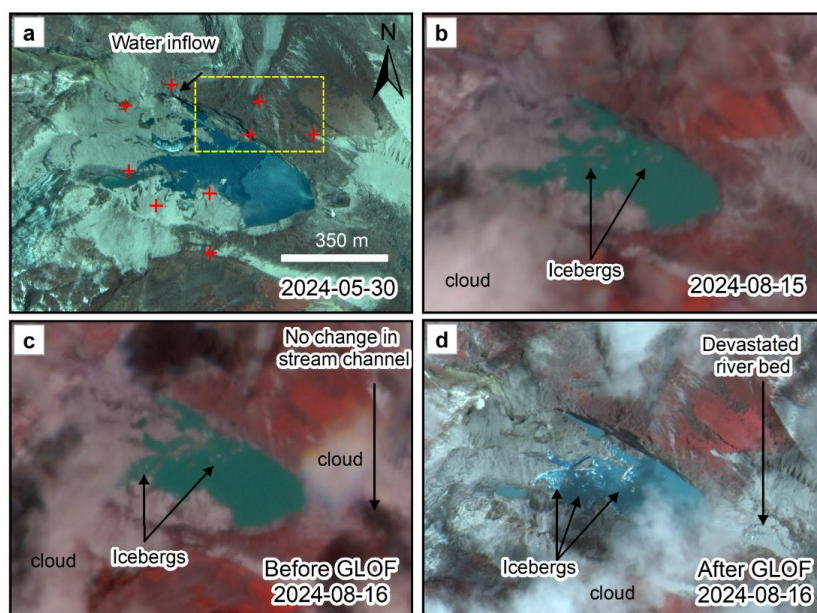


287

288 **Table 5. Analysis of different conditioning and triggering factors of the cascading GLOF.**

Conditioning and triggering factors analysed	Upper lake	Lower lake	Analysis and remarks
Ice-snow avalanche	Not evident	Not applicable	Immediate field observations by government institutions and Sagarmatha Pollution Control Committee
Rockfall or landslides	Not confirmed through high resolution images and geomorphological interpretation	Not applicable	Field observation shows the deposits of probable rockfall on the north zone; however, these appear weathered and old. Further, according to locals and satellite images, the rockfall deposits were there long before the GLOF (Fig. S5). Additionally, high-resolution Gaofen-7 imagery (0.65 m) and visible geology shows no signs of rock fall immediately prior to the GLOF (Fig. 4).
Calving of glacier or glacier retreat	Evident	Not applicable	Evidence of a wide calving front, large and numerous icebergs visible on Planet and Gaofen-7 satellite images
Lake size/volume increment	Evident	Not evident	Analysis of multi-source remote sensing images
Dead ice melting	No dead ice present	No dead ice present	Field and satellite image observation
Prior days with extreme temperature	Evident	Evident	Analysis of ERA5-Land datasets and interview with locals
Prior days with extreme precipitation	Evident	Evident	Evident from analysis of ERA-5 Land data
Seismicity	Not evident	Not evident	Not recorded
Permafrost degradation at dam sites	Not evident	Not evident	Not expected below 5000 m according to Singh et al. (2025)
Upper lake outburst	Not evident	Evident	Remote sensing analysis

289



290

291 **Figure 5: Monitoring changes in upper lake and surroundings before and after the GLOF. The red plus points indicate control**  
 292 **points used for monitoring the changes in land surface. The yellow dashed box shows a zone of rockfall with no visible change.**  
 293 **The image (c) is sensed on the same day just prior to the GLOF, reveals no sign of mass movement into the lake but formation**

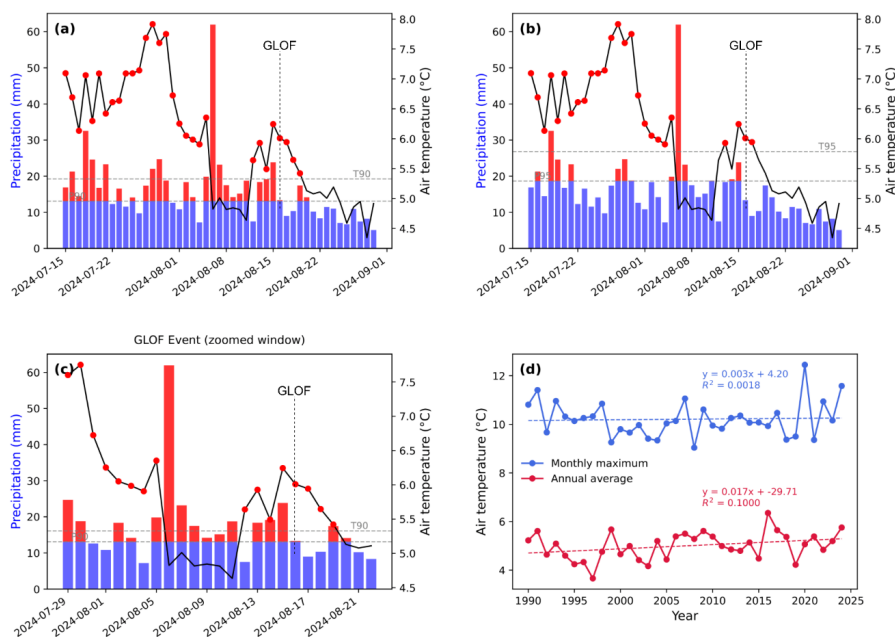


294 of icebergs due to calving. Background images (a) and (d) are sourced from Gaofen-2/7, whereas (b) and (d) are from  
295 PlanetScope. The figure was created by authors using ArcGIS® software by Esri.

#### 296 4.3 Meteorological analysis

297 In the month leading up to the occurrence of the GLOF, an analysis of the climate data revealed that several days  
298 experienced temperatures and precipitation levels that exceeded the 90<sup>th</sup> and 95<sup>th</sup> percentiles compared to long-term  
299 (1990–2024) average climatology (Fig. 6). This indicates a period of extreme weather conditions coinciding with a  
300 GLOF event. During summer months (JJAS), climate gets warmer and wetter than preceding autumn season (MAM) in  
301 Nepal. Specifically, the temperatures on August 12–15 prior to the GLOF event on August 16, surpassed both the 90<sup>th</sup>  
302 and 95<sup>th</sup> percentiles. Moreover, the precipitation on August 14 and 15 also exceeded both 90<sup>th</sup> and 95<sup>th</sup> percentiles (Fig.  
303 6a and b). Similarly, the preceding month July had experienced extreme temperatures and precipitation exceeding both  
304 90<sup>th</sup> and 95<sup>th</sup> percentiles. Extreme deviations in temperature and precipitation suggest that climate conditions were  
305 markedly warmer and wetter than historical averages for the region. This phenomenon likely contributed to accelerated  
306 glacier melt and a corresponding rise in lake volumes due to increased precipitation and enhanced ice loss in the upper  
307 lake.

308 The average annual temperature and the maximum monthly temperature during the summer seasons in the lake region  
309 have been observed to be increasing at rates of 0.015 °C and 0.003 °C per year, respectively, between 1990 and 2014  
310 (Fig. 6d). On the day preceding the outburst, the ERA5-Land data recorded minimum and maximum temperatures of 3.7  
311 °C and 9.7 °C, respectively with consecutive extreme wet days exceeding 10 days (Fig. 6c). Concurrently, data collected  
312 from the Phortse automatic weather station, located 11 km east at an elevation of 3,850 m, reported minimum and  
313 maximum temperatures of 7.45 °C and 14.13 °C, respectively, along with a total rainfall of 124 mm over a consecutive  
314 14-days wet period prior to the GLOF event (Fig. S6). This implies that the data of ERA5-Land, though being reanalysis,  
315 captures the general climatic conditions and trends of the region (Chen et al., 2021). These climatic conditions are  
316 conducive to increased glacier and snow melt, which might have been contributed glacier melt and calving, and initiation  
317 of the GLOF.



318

319 **Fig. 6: Meteorological conditions of the lake region. (a) Extreme air temperature and precipitation values (red colour) before the GLOF event exceeding the 90<sup>th</sup> percentile (a) and 95<sup>th</sup> percentile (b) compared to long term (1990-2024) average climatology, a zoomed view (c) for enhanced reading and (d) the trends of annual average temperature and maximum monthly temperature of that year from 1990 to 2024.**  
 320  
 321  
 322

#### 323 4.4 Cascading GLOF reconstruction

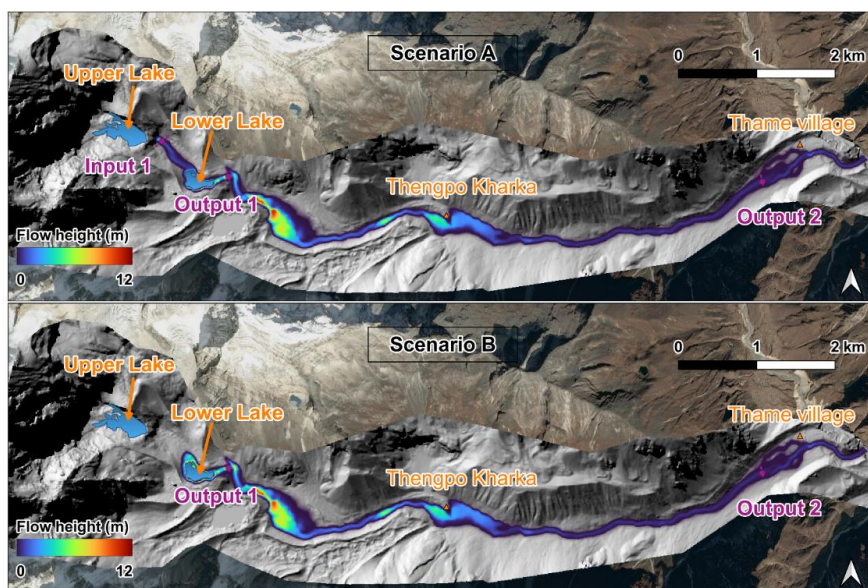
324 The reconstructed GLOF flow heights, arrival times, hydrographs and velocity for both scenarios A and B are shown in  
 325 Figs. 7, 8, 9 and S7. Accuracy assessment of reconstructed GLOF inundation areas show that Scenario A achieved  
 326 precision, recall, and F1 scores of 0.73, 0.85, and 0.78, respectively, while Scenario B yielded 0.71, 0.83, and 0.77.  
 327 Overall, these metrics indicate acceptable model performance in capturing the actual flood extent, with Scenario A being  
 328 more precise than Scenario B.

329 In Scenario A, the simulation results reveal the dynamic characteristics of the event and its downstream impacts. The  
 330 inflow hydrograph of the upstream lake (Fig. S3) exhibits a sharp peak of approximately 442 m<sup>3</sup>/s within 550 s. This  
 331 surge wave with velocities 15 m/s, released from Input1, first impacted the downstream lake, initiating its breach and  
 332 generating a compound flood. At the immediate downstream outlet (O1), the discharge hydrograph displays multiple  
 333 peaks exceeding 800 m<sup>3</sup>/s and lasting for more than 2000 s, reflecting a complex breach evolution process (Figure 9a). At  
 334 720 s after the breach, the liquid-phase discharge at O1 reached a peak of 900 m<sup>3</sup>/s, accompanied by the release of solid-  
 335 phase material derived from the erosion of the dam body during failure. The combined flood wave then propagated  
 336 downstream, reaching Thame Village (O2) 1,884 s (approximately 31.4 min, Figure 8) after the initial breach with  
 337 maximum flow heights up to 4 m and velocity of 10 m/s (Figure 7). Although significant channel storage effects and  
 338 energy dissipation reduced the peak discharge at O2 to approximately 200 m<sup>3</sup>/s, the magnitude and duration of the flood  
 339 remained sufficient with depositions to cause severe damage, highlighting the long-term hazard posed by cascading  
 340 GLOF events.



341 In Scenario B, in contrast to the sudden displacement wave in Scenario A, the failure was induced by sustained inflow  
342 from the upstream lake, which progressively increased the storage and water level of the downstream lake until  
343 overtopping and structural collapse occurred. The hydrographs illustrate the dynamic features of this breach mode. The  
344 discharge at O1 (breach output 1) shows a rapid rise to peak flow, a characteristic feature of dam-break floods, followed  
345 by gradual recession (Figure 9b). At 180 s after the breach, the liquid-phase discharge at O1 reached a peak of 1,050  
346 m<sup>3</sup>/s, accompanied by the outflow of solid-phase material originating from the dam body. The discharge at O2 (Thame  
347 Village) exhibits a delayed and attenuated yet still significant flood wave, arriving 1,340 s (22.3 min) after the breach  
348 with flow heights up to 4 m. This scenario highlights a comparatively slower-onset but high-volume failure process  
349 primarily driven by cumulative basin filling rather than instantaneous impact, resulting in a distinct hydrograph shape,  
350 lower travel time and potentially different downstream impacts compared with displacement-wave-triggered events.

351 Field observations reveal that a sand plain located immediately downstream of Thengpo Kharka, approximately 500 m  
352 long and 150 m wide, temporarily stored ponded water during the event (Fig. S8). Water released during GLOF event  
353 was briefly impounded within this sand plain, which likely attenuated the flood wave and delayed its downstream  
354 propagation. This phenomenon is accurately captured by the GLOF modelling, where water is shown to have been  
355 impounded just downstream of Thengpo Kharka (Figure 7). This temporary storage provided critical lead time for  
356 residents of Thame Village to evacuate safely. Subsequently, the impounded water overtopped and eroded the banks and  
357 bed of the ~2 km long channel between the ancient landslide dam and the debris fan near Thame Village, contributing to  
358 significant channel incision and sediment transport (Fig. S9).



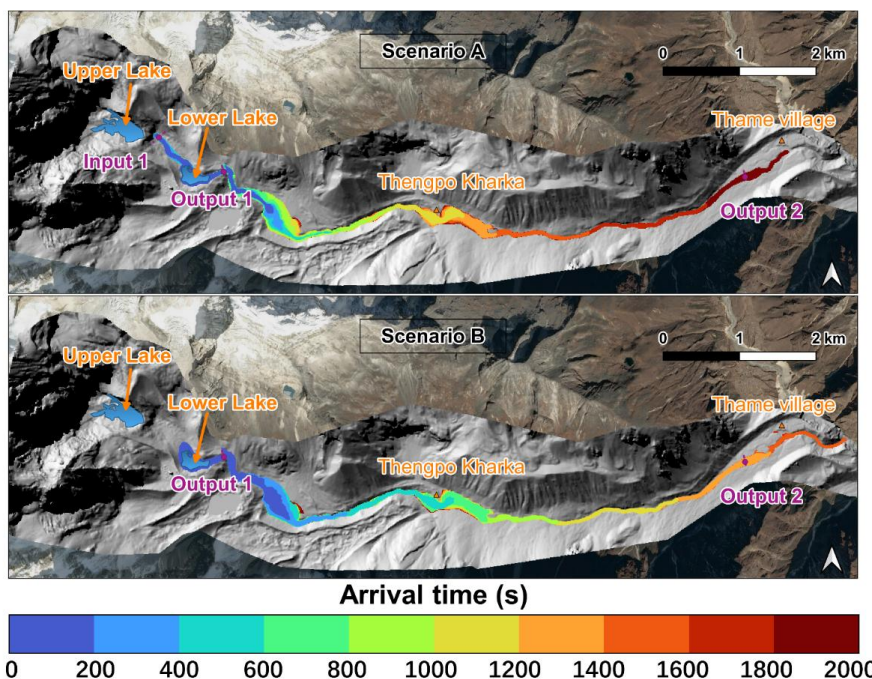
359

360

361

Figure 7: Simulation results of flow height (m) inundation for Scenario A and Scenario B. The figure was created by authors using QGIS and the background images are hill shade of HMA-DEM and the base images © Yandex.

362



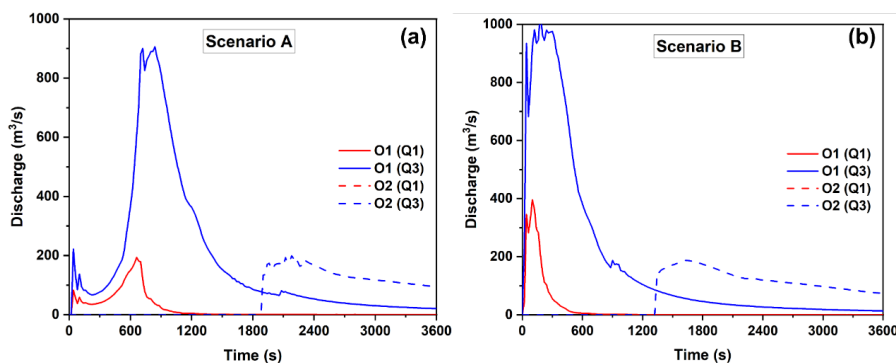
363

364

365

Figure 8: Simulation results of arrival times for Scenario A and Scenario B. The figure was created by authors using QGIS and the background images are hill shade of HMA-DEM and the base images © Yandex.

366



367

368

Figure 9: Hydrographs for Scenario A and Scenario B. Here, Q1 is Solid phase and Q3 is fluid phase.

#### 369 4.5 Downstream impacts of GLOF

370 The GLOF had profound impacts in the downstream areas as it turned into perilous debris flood with Thame Village  
 371 being the primary deposition zone (Figure 10 and S9). The roaring sound of the flood and information flow from  
 372 upstream to downstream areas helped the communities to evacuate during the GLOF event, leaving no casualties. The  
 373 GLOF had a devastating impact on Thame Village, displacing 135 people and leading to the destruction of several tea  
 374 houses and buildings, including the primary school, as well as considerable damage to agricultural fields (Figure 10). The  
 375 detailed impact assessment shows that GLOF impacted the settlements, trekking trails, land and infrastructures worth



376 total of 6.18 million USD in KPL RM alone (Table 6). The impacts of the GLOF were minimal outside the KPL RM;  
 377 however, it caused substantial erosion and bank cutting up to 50 kilometres downstream and partially damaged a  
 378 motorable bridge (Figure 10f).

379 The GLOF-triggered landslides in the Thame area, characterized by active glacio-lacustrine deposits, are ongoing. Deep-  
 380 seated movement in Thame Village is exacerbated by riverbank erosion and migration (Fig. S10), leading to persistent  
 381 ground settlement and tension cracking, particularly during wet periods. Elevated water levels during the monsoon  
 382 further destabilize the slopes, with landslide activity expected to extend into areas farther from the river. Deep-seated  
 383 rotational landslides are advancing from the east and north sides of the head pond on the right bank, impacting houses  
 384 and agricultural land on the left bank.

385

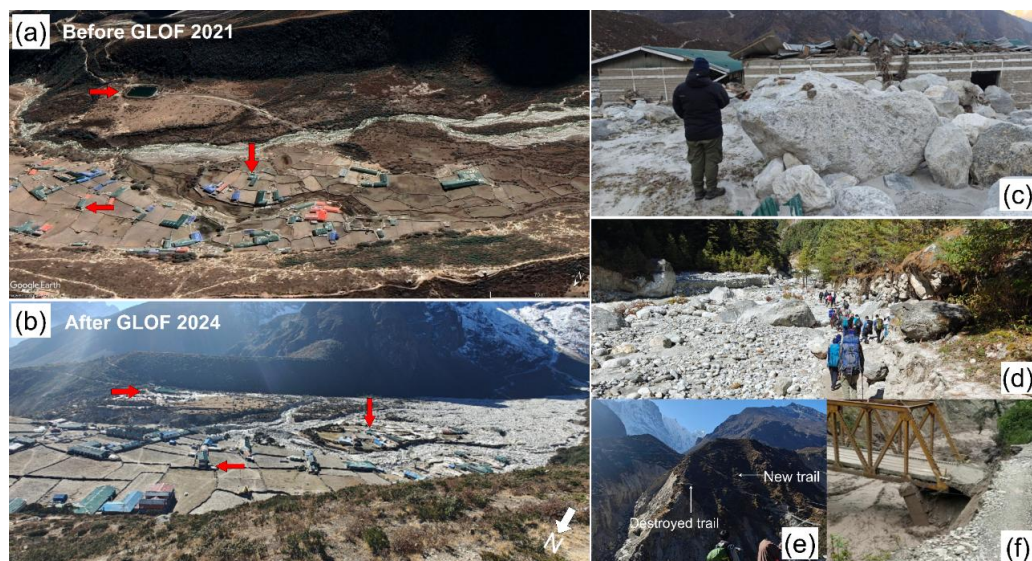
386 **Table 6. Impacts of GLOF on Khumbu Pashunglamu Rural Municipality.**

Items	Loss description	Monetary amount*	Remarks
People	1 injured	-	No casualties; 135 displaced
Buildings Private house + Lodge + 1 primary school	45 owners	NRs. 560,874,214 USD 4,185,316	Loss including buildings, furniture and property inside
	1 School	NRs. 60,050,000 USD 448,101	Including school properties without land evaluation
Trekking Trails	1.7 km in different places	NRs. 3,019,382 USD 22,531	Damaged and maintenance costs
Private land	98920 m <sup>2</sup>	204,847,183 USD 1,528,596	This includes agricultural and land property where there were buildings.
Micro-hydropower	Partial damage	-	The intake to desander and the pipes connecting them were damaged and was soon reconstructed and now is in operation
Bridges#	1	-	Motorable bridge was damaged 47 km downstream of Thame
Total		NRs. 82,879,780 USD 6,184,544	

387 #Outside KPL RM; \*Exchange rate of 1 USD = NRs 134.01 based on Nepal Central Bank's 2024-08-18 rate

388 (<https://www.nrb.org.np/forex/>)

389



390

391 **Figure 10: Impacts of Thame Valley GLOF. Thame Valley (a) before and (b) after GLOF, (c) the damaged Thame school,**  
392 **walking trails (d and e) and the motorable bridge (f). The red arrows show common feature/buildings on panels (a) and (b).**  
393 **Source: The picture (a) is sourced from © Google Earth 2024; images: © CNES/Airbus, Maxar Technologies, Airbus whereas**  
394 **others from Field Study, 2024.**

## 395 5 Discussion

### 396 5.1 Evolution of glacial lake attribution to climate change induced glacier retreat

397 Increase in temperatures in the Himalayan region are driving the retreat and mass loss of glacier (Bhattacharya et al.,  
398 2021) and subsequently new lakes are being emerged at higher elevation (>4,600 m a.s.l) in the Himalaya, including  
399 Nepal (Khadka et al., 2018). It is clearly visible in the satellite image that there is no existence of the upper lake before  
400 2000 (Figure 3a). In the eastern Nepal including Everest region, maximum annual temperature has increased by 0.06°C  
401 per year (Salerno et al., 2015) and particularly, in the study area, the annual average temperature has increased by 0.17  
402 °C per decade during 1994–2024 (Fig. 6d). In response to climatic warming, glaciers have retreated with rates of  
403  $-6.1 \pm 0.2 \text{ m yr}^{-1}$  between 1962 and 2011 (Thakuri et al., 2014). The parent glacier of the upper lake has shrunk by  $-0.45$   
404  $\text{km}^2$  between 1980 and 2024 (Figure 3a), consequently the lake started to develop as glacier mass loss accelerated. After  
405 the development of the glacial lake, pronounced lake-glacier interaction has resulted in upward proglacial lake expansion  
406 (Fig. S4).

### 407 5.2 Potential triggering factors of the upper lake outburst

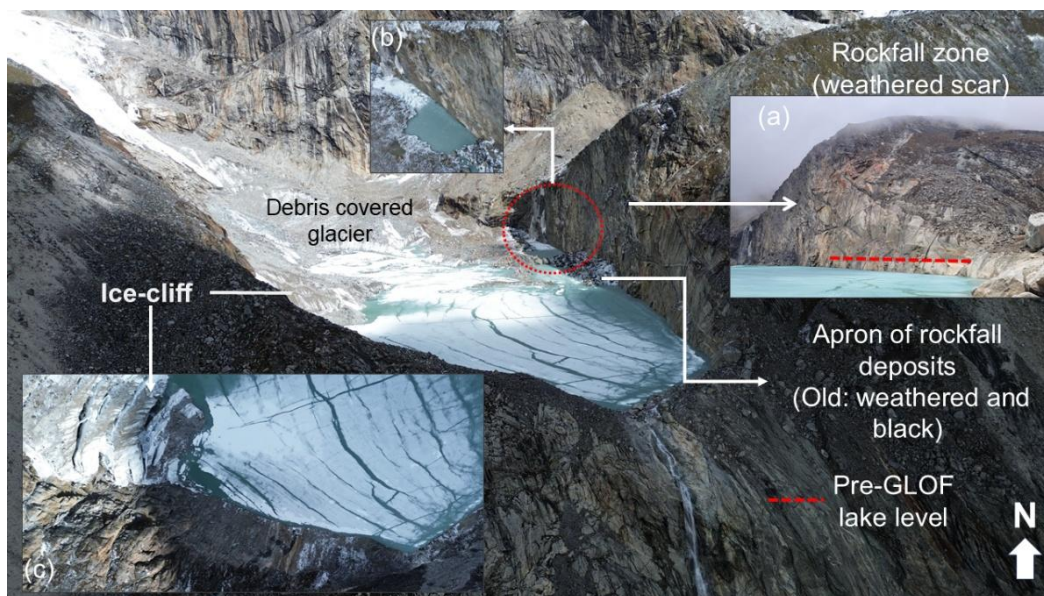
408 Although mass movements (e.g., snow/ice avalanches, rockfalls, or landslides) trigger over 70 % of Himalayan GLOFs  
409 (Nie et al., 2018; Lützwow et al., 2023), a probable snow/ice avalanche trigger was neither reported by government  
410 institutions or the Sagarmatha Pollution Control Committee during their immediate post-event field survey (Maharjan et  
411 al., 2025), nor was it evident in available remote sensing imagery. Through discounting other potential triggers (Table 5),  
412 our analysis indicates that the GLOF from upper lake was likely triggered by a rapid increase in lake volume, driven by  
413 extreme temperature-induced snow and glacier melt. The GLOF initiation potentially including calving from the parent



414 glacier, although it is possible this calving occurred post-GLOF caused by the lake level lowering. This interpretation  
415 contrasts with previously proposed trigger involving a recent rockfall as reported by ICIMOD (Maharjan et al., 2025).

416 High-resolution remote sensing images (Figure 5) and geomorphological/geological interpretation provides no clear  
417 evidence of a contemporary rockfall or rockslides (Figure 11a) impacting the lake. The rock deposits observed along the  
418 eastern moraine margins are characterized by a dark, weathered appearance, inconsistent with the fresh, sandy or whitish  
419 talus typically associated with recent rock avalanches (Figure 11). Historical imagery and local accounts confirm these  
420 deposits were likely pre-existing (Fig. S5). All historical images (Fig. S5) depict a cluster of boulders that has been  
421 present since 2014. It appears that this section of the rockfall is partially situated on debris-covered ice that is melting,  
422 rather than directly on the lake bed. Furthermore, fresh small patches of scars observed in the north-eastern zone are an  
423 unlikely source for the GLOF (Figure 11b). The corresponding rockfall volume appears too small to generate a  
424 displacement wave capable of significantly impacting the main lake. Even if a wave were generated, the narrow strait  
425 would dampen its energy before it could propagate into the main lake. Additionally, the extreme verticality of the terrain  
426 limits the reliability of DEM differencing for detecting recent slope failures. Even if a rockfall had occurred as described  
427 by Maharjan et al. (2025), its direct impact on the lake is considered unlikely as a substantial already present debris apron  
428 (~20–30 m wide) buffers the lake from the lateral moraine slopes, intercepting material and preventing a direct, dynamic  
429 hit on the water body.

430 Therefore, we conclude that the GLOF from upper lake was most likely caused by a hydrological tipping point, a  
431 phenomenon that similarly contributed to the 2013 Kedarnath outburst-related disaster (Allen et al., 2016) and the 2009  
432 outburst of Ventisquero Negro in the Patagonian Andes (Worni et al., 2012). Consecutive days of extreme precipitation  
433 and anomalously high temperatures prior to the event (Fig. 6) promoted intense meltwater generation and glacier calving  
434 (Figs. 5 and 11c). This rapid influx of water elevated the lake volume, ultimately exceeding the stability threshold of the  
435 moraine dam and culminating in the outburst. Notably, the cascading GLOF modelling, through its two scenarios  
436 effectively captures the range of possible outburst mechanisms and process (Sections 3.4 and 4.4), even when the exact  
437 triggering factor of the upper lake remains undefined.



438

439

Figure 11: Bird eye view of upper lake with surrounding geology captured on May 2025. Photos: C. S. Watson, 2025

### 440 5.3 Limitations of the modelling and study

441 One of the limitations of the study is the empirical quantification of lake volume, peak discharge and breach time since  
442 bathymetry and real time data are unavailable. Such empirical estimations might be under or overestimated but are used  
443 widely in the literature in the data scarce mountainous region (Zheng et al., 2021a; Zhang et al., 2025). Interestingly, the  
444 reconstructed drainage volume for the lower lake, which integrates post-GLOF bathymetry and DEM, shows close  
445 agreement with the empirical estimates, thereby supporting the reliability of the empirical approach used in this study  
446 (Text S1). The absence of high-resolution DEMs for the post-GLOF period precluded the incorporation of spatially  
447 heterogeneous parameter values and constrained the calibration of model inputs (Zhang et al., 2025). Consequently, the  
448 discharge and the simulated results by the model might be underestimated, particularly in the Thame Valley as compared  
449 to field—limitations attributable to the lack of fine resolution DEM, post-event topographic data and uncertainties  
450 associated with erosion (including large boulders) and deposition rates along the river channel (Fig. S9). This limitation  
451 is consistent with previously documented challenges in r.avaflow applications or any hydrodynamic models (Rinzin et  
452 al., 2025; Sattar et al., 2025). Moreover, r.avaflow is sensitive to input parameters and adjusting them can affect mass  
453 flow behaviour (Mergili et al., 2018a). Future modelling studies can enhance debris flow dynamics by incorporating  
454 high-resolution DEMs along with erosion and deposition rates along the river channel. While alternative hydrodynamic  
455 models such as HEC-RAS may offer advantages in accurately reproducing inundation extents (Sattar et al., 2025),  
456 metrics such as travel time and peak discharge are of greater relevance in the context of complex mass flows and  
457 cascading processes (Mergili et al., 2020a). In this regard, the performance of r.avaflow remains satisfactory and also the  
458 inundation extent produced by it when compared to post-GLOF images with acceptable F1 scores (Figure 7 vs Fig. S9).  
459 The GLOF modelling is limited to Thame Village; therefore, future studies could assess GLOF impacts further  
460 downstream.



461 On the impacts side, tangible loss is quantified in this study however intangible impacts and losses such as cultural loss,  
462 mental and physical stress of GLOF is not covered by this study and needs a different evaluation and assessment  
463 approach.

#### 464 **5.4 Future GLOF hazard of upper and lower glacial lake**

465 GLOF hazard refers to the likelihood and magnitude of an outburst event from a given lake, considering a broad range of  
466 contributing factors (Allen et al., 2022). In this context, both national (Rounce et al., 2017) and basin scale (Khadka et  
467 al., 2021) hazard assessments have overlooked the upper and lower lakes, primarily due to minimum size thresholds used  
468 in their studies (Table 1). To address this gap, a first-order assessment of future GLOF hazard for both lakes was  
469 systematically conducted by analysing twenty GLOF hazard factors (Gaphaz, 2017) that encompass atmospheric,  
470 cryospheric, geotechnical and geomorphological, conditioning and triggering variables (Table S4).

471 Expert evaluation indicates that a repeated GLOF from the upper lake is possible. The lake remains connected to a  
472 calving glacier, has potential to expand and is highly susceptible to ice/snow avalanches and rockfall (Figure 11).  
473 However, since much of the moraine and debris comprising the dam was removed by the recent GLOF, the upper lake is  
474 less susceptible to dynamic failure processes since the lake is bedrock-dammed. However, overtopping from  
475 displacement waves could still occur as most of the upper lake volume remains. In contrast, the lower lake has been  
476 substantially reduced in volume (by ~80%, Table S1) by the recent event. It no longer has direct contact with a glacier  
477 (Figure 1) and is not susceptible to direct ice- or rock-fall triggers. However, it remains susceptible to a potential outburst  
478 if a GLOF from the upper lake were to occur. Thus, regular monitoring of upper glacial lake is recommended using  
479 remote sensing technologies and field assessments.

#### 480 **5.5 Disaster risk management in Thame Valley**

481 The Thame GLOF event underscores the need for proactive, integrated disaster risk management that addresses  
482 compound hazards in the Thame Valley, including glacio-lacustrine landslides, monsoon-driven flooding, channel  
483 instability, and potential future GLOFs from small lakes. Risk in the valley arises not only from the probability of  
484 extreme outburst floods but also from the interaction of ongoing geomorphic processes with settlements and critical  
485 infrastructure along the Thame stream (Fig. S10). Effective risk management must therefore integrate hazard assessment,  
486 exposure reduction, and vulnerability mitigation within a unified framework (Niggli et al., 2024).

487 Short-term measures should focus on reducing hazard impacts and immediate exposure rather than attempting to  
488 eliminate underlying geomorphic drivers. Targeted structural interventions—such as selective, over-toppable flow-  
489 diversion berms near the debris-fan apex and localized bank protection within the village—can help limit flood intrusion  
490 and channel migration under recurrent monsoon conditions. Concurrently, GLOF exposure and vulnerability must be  
491 reduced through land-use restrictions or zoning, evacuation of structurally compromised buildings and systematic ground  
492 deformation monitoring. Low-cost monitoring approaches can support adaptive decision-making, including evacuation  
493 thresholds and infrastructure relocation, while large-scale river engineering works are not recommended due to high cost,  
494 technical uncertainty, and limited long-term effectiveness.

495 Over the long term, sustainable GLOF risk reduction depends primarily on exposure management through risk-informed  
496 land-use planning and the progressive relocation of permanent settlements and critical infrastructure to lower-hazard



497 zones (Khadka et al., 2024a). Areas subject to frequent flooding or landsliding should be reserved for low-exposure  
498 areas. Given persistent residual risk, a robust GLOF early warning system is also essential to reduce vulnerability and  
499 prevent loss of life. Such a system must combine reliable hydrological monitoring, redundant communication  
500 mechanisms, clear evacuation planning, and strong institutional support for maintenance and periodic reassessment  
501 (Wang et al., 2026). Overall, the Thame case highlights that in high-mountain environments, reducing GLOF exposure  
502 and vulnerability is more effective than attempting to fully control dynamic geomorphic hazards and implementing  
503 expensive lake mitigation projects such as lake lowering.

## 504 **6 Conclusions**

505 This study provides a comprehensive analysis of the cascading GLOF event in the Thame Valley on August 16, 2024, an  
506 event originating from relatively small, often overlooked, glacial lakes in the headwaters. By integrating multi-source  
507 remote sensing, climatic data, numerical modelling, field assessments, and government reports, we reconstructed and  
508 evaluated the process chain of this event, potential mechanisms, and downstream impacts.

509 Our findings reveal that the GLOF was a direct consequence of rapid and ongoing cryospheric change. The upper glacial  
510 lake experienced significant expansion in recent years due to climate-induced glacier retreat. The immediate trigger for  
511 its outburst was likely extremes of temperature and precipitation, surpassing the 90<sup>th</sup> and 95<sup>th</sup> percentiles of historical  
512 records, which drove rapid melt and ice-calving into the lake. This initial failure released a flood that, in turn, breached  
513 the lower glacial lake, creating a cascading GLOF process. A combined volume of approximately  $6 \times 10^5$  m<sup>3</sup> of water  
514 was released. Post-event, the surface area of the upper lake decreased by 0.013 km<sup>2</sup>, while the lower lake was reduced  
515 from  $0.048 \pm 0.01$  km<sup>2</sup> to 0.015 km<sup>2</sup>.

516 Numerical modelling using the r.avaflo mass flow model, which considered two likely scenarios, successfully  
517 reconstructed the event dynamics. The simulation indicates that the heterogeneous flood wave height reaching maximum  
518 up to 12 m height along the river channel. The flood wave reached Thame Valley within 22 to 32 minutes of the initial  
519 outburst, transitioning into a highly destructive debris flow as it propagated downstream. Although no casualties were  
520 reported, the socio-economic impact was substantial, causing an estimated 6.18 million USD in damage to settlements,  
521 trekking routes, and infrastructure in 2024.

522 The Thame Valley event reveals a critical gap in current GLOF risk assessment paradigms: the underestimated hazard of  
523 rapidly evolving small high-mountain lakes, particularly when they form cascading systems along a single channel. This  
524 disaster exemplifies the direct linkage between climate change, glacier retreat, and the generation of downstream  
525 hazards. Consequently, we argue for a strategic shift in risk management. In such dynamic high-mountain environments,  
526 priority should be given to reducing the exposure and vulnerability of downstream communities and infrastructure, rather  
527 than focusing solely on the technically challenging and often ineffective task of mitigating GLOFs at their source or  
528 attempting to control the geomorphic hazards themselves. Future GLOF risk assessments should therefore prioritize the  
529 systematic monitoring of all glacial lakes, regardless of size, as well as settlements located along river channels that may  
530 be vulnerable to cascading events.

531



532 **Supplement.** The supplement related to this article has been submitted for review.

#### 533 **Code and Data availability**

534 The mass flow simulation tool, `r.avaflow` used for GLOF modelling is freely available at  
535 <https://www.landslidemodels.org/r.avaflow/> (Mergili and Pudasaini, 2014-2025). Landsat data is sourced from  
536 <https://earthexplorer.usgs.gov/>, Sentinel-2 from <https://browser.dataspace.copernicus.eu/> and HMA DEM from  
537 <https://nsidc.org/data/> whereas ERA5-Land data are obtained from Google Earth Engine  
538 (<https://earthengine.google.com>). The ice thickness data was obtained from <https://doi.org/10.3929/ethz-b-000315707>.  
539 Additional commercial and closed access datasets used are available from the corresponding or lead authors on request.

#### 540 **Author contributions**

541 NK and VPP developed the idea with inputs from GZ. NK, KS, and CSW conducted field studies differently in October-  
542 December 2024 and May 2025. NK collected required data from GZ, CSW, KB, and DB. NK developed the manuscript  
543 with inputs from TW in the GLOF simulations and under supervision of VPP. All authors contributed in the discussion,  
544 revision and editing of the manuscript and approved the final draft.

#### 545 **Competing interests**

546 The authors declare that they have no conflict of interest.

#### 547 **Acknowledgement**

548 The authors would like to acknowledge ‘ReCAP - Developing MH risk assessment model and supporting the design of  
549 MHEWS approach in Nepal’ project funded by SDC as well as ‘Collaborative Research and Capacity Strengthening for  
550 Enhancing Water Security (CaREWaS)’ project funded by Kathmandu Valley Water Supply Management Board for  
551 supporting NK, VPP and SA. Further, it builds on the field study to Thame on October-Novemembr 2024 supported by  
552 IMHE-CAS to NK. The contribution of GZ was supported by the National Natural Science Foundation of China  
553 (42301140, 42571150) and the National Key Research and Development Program of China (2024YFF0808603). KS  
554 gratefully acknowledges the support of the Asian Development Bank (ADB) and NDRRMA, Nepal in facilitating the  
555 field visit to Thame under the Building Adaptation and Resilience in the Hindu Kush Himalaya (BARHKH) project. NK  
556 thanks Archana Ghimire (KPL RM Environment officer) for her help. The language of some sections was polished and  
557 Figure 2a was converted to 3D using ChatGPT.

#### 558 **References**

- 559 Allen, S. K., Rastner, P., Arora, M., Huggel, C., and Stoffel, M.: Lake outburst and debris flow disaster at Kedarnath,  
560 June 2013: hydrometeorological triggering and topographic predisposition, *Landslides*, 13, 1479-1491,  
561 <https://doi.org/10.1007/s10346-015-0584-3>, 2016.
- 562 Allen, S. K., Zhang, G., Wang, W., Yao, T., and Bolch, T.: Potentially dangerous glacial lakes across the Tibetan Plateau  
563 revealed using a large-scale automated assessment approach, *Sci Bull*, 64, 435-445,  
564 <https://doi.org/10.1016/j.scib.2019.03.011>, 2019.



- 565 Allen, S. K., Sattar, A., King, O., Zhang, G., Bhattacharya, A., Yao, T., and Bolch, T.: Glacial lake outburst flood hazard  
566 under current and future conditions: worst-case scenarios in a transboundary Himalayan basin, *Natural Hazards and*  
567 *Earth System Sciences*, 22, 3765-3785, <https://doi.org/10.5194/nhess-22-3765-2022>, 2022.
- 568 Bajracharya, S. R., Shrestha, A. B., Shrestha, F., Wagle, N., Maharjan, S. B., and Sherpa, T. C.: Inventory of glacial lakes  
569 and identification of potentially dangerous glacial lakes in the Koshi, Gandaki, and Karnali river basins of Nepal,  
570 the Tibet autonomous region of China, and India, *International Centre for Integrated Mountain Development*  
571 *(ICIMOD); United Nations Development Programme (UNDP), Kathmandu, Nepal*, 54, 10.53055/ICIMOD.773,  
572 2020.
- 573 Bhattacharya, A., Bolch, T., Mukherjee, K., King, O., Menounos, B., Kapitsa, V., Neckel, N., Yang, W., and Yao, T.: High  
574 Mountain Asian glacier response to climate revealed by multi-temporal satellite observations since the 1960s,  
575 *Nature communications*, 12, 4133, <https://doi.org/10.1038/s41467-021-24180-y>, 2021.
- 576 Byers, A. C.: Khumbu since 1950: cultural, landscape, and climate change in the Sagarmatha (Mt. Everest) National  
577 Park, Khumbu, Nepal, *Alton C. Byers*2017.
- 578 Byers, A. C., Rounce, D. R., Shugar, D. H., Lala, J. M., Byers, E. A., and Regmi, D.: A rockfall-induced glacial lake  
579 outburst flood, Upper Barun Valley, Nepal, *Landslides*, 1-17, <https://doi.org/10.1007/s10346-018-1079-9>, 2018.
- 580 Chen, H., Liang, Q., Zhao, J., and Maharjan, S. B.: Assessing national exposure to and impact of glacial lake outburst  
581 floods considering uncertainty under data sparsity, *Hydrol. Earth Syst. Sci.*, 29, 733-752, 10.5194/hess-29-733-  
582 2025, 2025.
- 583 Chen, H., Wu, T., Li, S., Chen, J., Ruan, H., Li, X., and Mou, Y.: New insights on the 2020 Jinwucuo glacial lake outburst  
584 flood: considering ice content within the moraine dam, *Geomatics, Natural Hazards and Risk*, 17, 2649567,  
585 10.1080/19475705.2026.2649567, 2026.
- 586 Chen, N., Liu, M., Allen, S., Deng, M., Khanal, N. R., Peng, T., Tian, S., Huggel, C., Wu, K., Rahman, M., and Somos-  
587 Valenzuela, M.: Small outbursts into big disasters: Earthquakes exacerbate climate-driven cascade processes of the  
588 glacial lakes failure in the Himalayas, *Geomorphology*, 422, 108539, 10.1016/j.geomorph.2022.108539, 2023.
- 589 Chen, Y., Sharma, S., Zhou, X., Yang, K., Li, X., Niu, X., Hu, X., and Khadka, N.: Spatial performance of multiple  
590 reanalysis precipitation datasets on the southern slope of central Himalaya, *Atmospheric Research*, 250, 105365,  
591 2021.
- 592 Cook, K. L., Andermann, C., Gimbert, F., Adhikari, B. R., and Hovius, N.: Glacial lake outburst floods as drivers of  
593 fluvial erosion in the Himalaya, *Science*, 362, 53-57, 2018.
- 594 Cook, S. and Quincey, D.: Estimating the volume of Alpine glacial lakes, *Earth Surface Dynamics*, 3, 559, 2015.
- 595 Costa, J. E.: Floods from dam failures, 560, *US Geological Survey*1985.
- 596 COSTA, J. E. and SCHUSTER, R. L.: The formation and failure of natural dams, *GSA Bulletin*, 100, 1054-1068,  
597 10.1130/0016-7606(1988)100<1054:TFAFON>2.3.CO;2 %J *GSA Bulletin*, 1988.
- 598 Cuellar, A. D. and McKinney, D. C.: Decision-Making Methodology for Risk Management Applied to Imja Lake in  
599 Nepal, *Water*, 9, 591, 2017.
- 600 Dubey, S. and Goyal, M. K.: Glacial Lake Outburst Flood Hazard, Downstream Impact, and Risk Over the Indian  
601 Himalayas, *Water Resources Research*, 56, e2019WR026533, 2020.
- 602 Evans, S. G.: The maximum discharge of outburst floods caused by the breaching of man-made and natural dams,  
603 *Canadian Geotechnical Journal*, 23, 385-387, 10.1139/t86-053, 1986.
- 604 Froehlich, D.: Predicting Peak Discharge of Outburst Floods from Moraine-Dammed Glacial Lakes, *Natural Hazards*  
605 *Review*, 26, 04025047, <https://doi.org/10.1061/NHREFO.NHENG-2492>, 2025.
- 606 Froehlich, D. C.: Peak outflow from breached embankment dam, *Journal of water Resources Planning and management*,  
607 121, 90-97, 1995.
- 608 Furian, W. and Sauter, T.: Assessing economic impacts of future GLOFs in Nepal's Everest region under different SSP  
609 scenarios using three-dimensional simulations, *Nat. Hazards Earth Syst. Sci.*, 25, 3779-3802,  
610 <https://doi.org/10.5194/nhess-25-3779-2025>, 2025.
- 611 Furian, W., Loibl, D., and Schneider, C.: Future glacial lakes in High Mountain Asia: an inventory and assessment of  
612 hazard potential from surrounding slopes, *Journal of Glaciology*, 67, 653-670, <https://doi.org/10.1017/jog.2021.18>,  
613 2021.
- 614 GAPHAZ: Assessment of Glacier and Permafrost Hazards in Mountain Regions – Technical Guidance Document. ,  
615 Zurich, Switzerland / Lima, Peru, , 72, 2017.



- 616 Ghimire, B.: Aerial inspection ties Thame flood to glacial lake outburst, The Kathmandu Post,  
617 [https://kathmandupost.com/climate-environment/2024/08/18/aerial-inspection-ties-thame-flood-to-glacial-lake-](https://kathmandupost.com/climate-environment/2024/08/18/aerial-inspection-ties-thame-flood-to-glacial-lake-outburst)  
618 outburst Last Accessed 05/04/2026, 2024.
- 619 Gouli, M. R., Hu, K., Khadka, N., Liu, S., Yifan, S., Adhikari, M., and Talchabhadel, R.: Quantitative assessment of the  
620 GLOF risk along China-Nepal transboundary basins by integrating remote sensing, machine learning, and  
621 hydrodynamic model, *International Journal of Disaster Risk Reduction*, 118, 105231, [10.1016/j.ijdr.2025.105231](https://doi.org/10.1016/j.ijdr.2025.105231),  
622 2025.
- 623 Hu, J., Yao, X., Duan, H., Zhang, Y., Wang, Y., and Wu, T.: Temporal and Spatial Changes and GLOF Susceptibility  
624 Assessment of Glacial Lakes in Nepal from 2000 to 2020, *Remote Sensing*, 14, 5034, 2022.
- 625 Huggel, C., Kääb, A., Haerberli, W., Teysseire, P., and Paul, F.: Remote sensing based assessment of hazards from glacier  
626 lake outbursts: a case study in the Swiss Alps, *Canadian Geotechnical Journal*, 39, 316-330, 2002.
- 627 ICIMOD: Glacial Lakes and Glacial Lake Outbursts Floods in Nepal ICIMOD, Kathmandu, 99, 2011.
- 628 Kapitsa, V., Shahgedanova, M., Machguth, H., Severson, I., and Medeu, A.: Assessment of evolution and risks of glacier  
629 lake outbursts in the Dzungarskiy Alatau, Central Asia, using Landsat imagery and glacier bed topography  
630 modelling, *Nat. Hazards Earth Syst. Sci.*, 17, 1837-1856, <https://doi.org/10.5194/nhess-17-1837-2017>, 2017.
- 631 Khadka, N., Zhang, G., and Chen, W.: The state of six dangerous glacial lakes in the Nepalese Himalaya, *Terr. Atmos.*  
632 *Ocean. Sci.*, 30, 63-72, 2019.
- 633 Khadka, N., Zhang, G., and Thakuri, S.: Glacial lakes in the Nepal Himalaya: Inventory and decadal dynamics (1977–  
634 2017), *Remote Sensing*, 10, 1913, <https://doi.org/10.3390/rs10121913>, 2018.
- 635 Khadka, N., Chen, X., Sharma, S., and Shrestha, B.: Climate change and its impacts on glaciers and glacial lakes in  
636 Nepal Himalayas, *Regional Environmental Change*, 23, 143, <https://doi.org/10.1007/s10113-023-02142-y>, 2023.
- 637 Khadka, N., Chen, X., Shrestha, M., and Liu, W.: Risk perception and vulnerability of communities in Nepal to  
638 transboundary glacial lake outburst floods from Tibet, China, *International Journal of Disaster Risk Reduction*, 107,  
639 104476, <https://doi.org/10.1016/j.ijdr.2024.104476>, 2024a.
- 640 Khadka, N., Chen, X., Yong, N., Thakuri, S., Zheng, G., and Zhang, G.: Evaluation of Glacial Lake Outburst Flood  
641 susceptibility using multi-criteria assessment framework in Mahalangur Himalaya, *Frontiers in Earth Science*, 8,  
642 748, <https://doi.org/10.3389/feart.2020.601288>, 2021.
- 643 Khadka, N., Zheng, G., Chen, X., Zhong, Y., Allen, S. K., and Gouli, M. R.: An ice-snow avalanche triggered small  
644 glacial lake outburst flood in Birendra Lake, Nepal Himalaya, *Natural Hazards*, 121, 6357-6365,  
645 <https://doi.org/10.1007/s11069-024-07014-0>, 2024b.
- 646 Khanal, N. R., Hu, J.-M., and Mool, P.: Glacial lake outburst flood risk in the Poiqu/Bhote Koshi/Sun Koshi river basin  
647 in the Central Himalayas, *Mountain Research and Development*, 35, 351-364, 2015.
- 648 King, O., Quincey, D. J., Carrivick, J. L., and Rowan, A. V.: Spatial variability in mass loss of glaciers in the Everest  
649 region, central Himalayas, between 2000 and 2015, *The Cryosphere*, 11, 407-426, 2017.
- 650 Lala, J. M., Rounce, D. R., and McKinney, D. C.: Modeling the glacial lake outburst flood process chain in the Nepal  
651 Himalaya: reassessing Imja Tsho's hazard, *Hydrology and Earth System Sciences*, 22, 3721-3737, 2018.
- 652 Lamsal, D., Sawagaki, T., Watanabe, T., Byers, A. C., and McKinney, D. C.: An assessment of conditions before and  
653 after the 1998 Tam Pokhari outburst in the Nepal Himalaya and an evaluation of the future outburst hazard,  
654 *Hydrological Processes*, 30, 676-691, 2016.
- 655 Lee, E., Carrivick, J. L., Quincey, D. J., Cook, S. J., James, W. H., and Brown, L. E.: Accelerated mass loss of Himalayan  
656 glaciers since the Little Ice Age, *Scientific reports*, 11, 24284, <https://doi.org/10.1038/s41598-021-03805-8>, 2021.
- 657 Lützwon, N., Veh, G., and Korup, O.: A global database of historic glacier lake outburst floods, *Earth System Science*  
658 *Data*, 15, 2983-3000, [10.5194/essd-15-2983-2023](https://doi.org/10.5194/essd-15-2983-2023), 2023.
- 659 Maharjan, S. B., Sherpa, T. C., and Shrestha, A. B.: Thame Valley Glacial Lake Outburst Flood 2024: Causes, impacts  
660 and future risks, ICIMOD, NDRRMA <https://doi.org/10.53055/ICIMOD.1101>, Kathmandu, 2025.
- 661 Majeed, U., Rashid, I., Sattar, A., Allen, S., Stoffel, M., Nüsser, M., and Schmidt, S.: Recession of Gya Glacier and the  
662 2014 glacial lake outburst flood in the Trans-Himalayan region of Ladakh, India, *Science of The Total*  
663 *Environment*, 756, 144008, 2021.
- 664 r. avaflow–The mass flow simulation tool <https://www.avaflow.org>, last  
665 Mergili, M., Fischer, J.-T., Krenn, J., and Pudasaini, S. P.: r. avaflow v1, an advanced open-source computational  
666 framework for the propagation and interaction of two-phase mass flows, *Geoscientific Model Development*, 10,  
667 553-569, <https://doi.org/10.5194/gmd-10-553-2017>, 2017.



- 668 Mergili, M., Jaboyedoff, M., Pullarello, J., and Pudasaini, S. P.: Back calculation of the 2017 Piz Cengalo–Bondo  
669 landslide cascade with r.avaflow: what we can do and what we can learn, *Nat. Hazards Earth Syst. Sci.*, 20, 505-  
670 520, 10.5194/nhess-20-505-2020, 2020a.
- 671 Mergili, M., Pfeffer, H., Kellner-Pirklbauer, A., Zangerl, C., and Pudasaini, S. P.: r.avaflow v4, a multi-purpose  
672 landslide simulation framework, *Geoscientific Model Development*, 18, 9879-9896, <https://doi.org/10.5194/gmd-18-9879-2025>, 2025.
- 673  
674 Mergili, M., Pudasaini, S. P., Emmer, A., Fischer, J.-T., Cochachin, A., and Frey, H.: Reconstruction of the 1941 GLOF  
675 process chain at lake Palcacocha (Cordillera Blanca, Peru), *Hydrology and Earth System Sciences*, 24, 93-114,  
676 2020b.
- 677 Mergili, M., Emmer, A., Juřicová, A., Cochachin, A., Fischer, J.-T., Huggel, C., and Pudasaini, S. P.: How well can we  
678 simulate complex hydro-geomorphic process chains? The 2012 multi-lake outburst flood in the Santa Cruz Valley  
679 (Cordillera Blanca, Perú), 43, 1373-1389, <https://doi.org/10.1002/esp.4318>, 2018a.
- 680 Mergili, M., Emmer, A., Juřicová, A., Cochachin, A., Fischer, J. T., Huggel, C., and Pudasaini, S. P.: How well can we  
681 simulate complex hydro-geomorphic process chains? The 2012 multi-lake outburst flood in the Santa Cruz Valley  
682 (Cordillera Blanca, Perú), *Earth surface processes and landforms*, 43, 1373-1389, <https://doi.org/10.1002/esp.4318>,  
683 2018b.
- 684 Muñoz-Sabater, J., Dutra, E., Agustí-Panareda, A., Albergel, C., Arduini, G., Balsamo, G., Boussetta, S., Choulga, M.,  
685 Harrigan, S., and Hersbach, H. J. E. s. s. d.: ERA5-Land: A state-of-the-art global reanalysis dataset for land  
686 applications, 13, 4349-4383, 2021.
- 687 National Statistic Office: National Population and Housing Census 2021 (National Report) National Statistic Office,  
688 Government of Nepal Kathmandu ([https://censusnepal.cbs.gov.np/results/files/result-  
689 folder/National%20Report\\_English.pdf](https://censusnepal.cbs.gov.np/results/files/result-folder/National%20Report_English.pdf)), 2023.
- 690 Nie, Y., Liu, W., Liu, Q., Hu, X., and Westoby, M. J.: Reconstructing the Chongbaxia Tsho glacial lake outburst flood in  
691 the Eastern Himalaya: Evolution, process and impacts, *Geomorphology*, 370, 107393, 2020.
- 692 Nie, Y., Liu, Q., Wang, J., Zhang, Y., Sheng, Y., and Liu, S.: An inventory of historical glacial lake outburst floods in the  
693 Himalayas based on remote sensing observations and geomorphological analysis, *Geomorphology*, 308, 91-106,  
694 2018.
- 695 Niggli, L., Allen, S., Frey, H., Huggel, C., Petrakov, D., Raimbekova, Z., Reynolds, J., and Wang, W.: GLOF Risk  
696 Management Experiences and Options: A Global Overview, 10.1093/acrefore/9780199389407.013.540, 2024.
- 697 Popov, N.: Assessment of glacial debris flow hazard in the north Tien-Shan, *Proceedings of the Soviet-China-Japan  
698 Symposium and field workshop on natural disasters*, 384-391,
- 699 Poudel, U., Gouli, M. R., Hu, K., Khadka, N., Regmi, R. K., and Thapa, B. R.: Multi-breach GLOF hazard and exposure  
700 analysis of Birendra Lake in the Manaslu Region of Nepal, *Natural Hazards Research*, 5, 800-813,  
701 10.1016/j.nhres.2025.03.007, 2025.
- 702 Pudasaini, S. P. and Mergili, M.: A multi-phase mass flow model, *Journal of Geophysical Research: Earth Surface*, 124,  
703 2920-2942, <https://doi.org/10.1029/2019JF005204>, 2019.
- 704 Rawlins, L. D., Watson, C. S., Bhambri, R., Khadka, N., and Chand, M. B.: Glacial Lake Observatory (GLO): Annual  
705 dataset of glacial lakes in Nepal and transboundary catchments (2017–2024), *Earth Syst. Sci. Data Discuss.*, 2026,  
706 1-33, 10.5194/essd-2025-751, 2026.
- 707 Rinzin, S., Dunning, S., Carr, R. J., Sattar, A., and Mergili, M.: Exploring implications of input parameter uncertainties in  
708 glacial lake outburst flood (GLOF) modelling results using the modelling code r.avaflow, *Nat. Hazards Earth Syst.  
709 Sci.*, 25, 1841-1864, 10.5194/nhess-25-1841-2025, 2025.
- 710 Rinzin, S., Zhang, G., Sattar, A., Wangchuk, S., Allen, S. K., Dunning, S., and Peng, M.: GLOF hazard, exposure,  
711 vulnerability, and risk assessment of potentially dangerous glacial lakes in the Bhutan Himalaya, *Journal of  
712 Hydrology*, 619, 129311, <https://doi.org/10.1016/j.jhydrol.2023.129311>, 2023.
- 713 Rounce, D. R., Watson, C. S., and McKinney, D. C.: Identification of hazard and risk for glacial lakes in the Nepal  
714 Himalaya using satellite imagery from 2000–2015, *Remote Sensing*, 9, 654, <https://doi.org/10.3390/rs9070654>,  
715 2017.
- 716 Sakai, A.: Glacial lakes in the Himalayas: a review on formation and expansion processes, *Global Environmental  
717 Research*, 16, 23-30, 2012.



- 718 Salerno, F., Thakuri, S., D'Agata, C., Smiraglia, C., Manfredi, E. C., Viviano, G., and Tartari, G.: Glacial lake  
719 distribution in the Mount Everest region: Uncertainty of measurement and conditions of formation, *Global and*  
720 *Planetary Change*, 92, 30-39, 2012.
- 721 Salerno, F., Guyennon, N., Thakuri, S., Viviano, G., Romano, E., Vuillermoz, E., Cristofanelli, P., Stocchi, P., Agrillo, G.,  
722 and Ma, Y.: Weak precipitation, warm winters and springs impact glaciers of south slopes of Mt. Everest (central  
723 Himalaya) in the last 2 decades (1994–2013), *The Cryosphere*, 9, 1229-1247, 2015.
- 724 Sattar, A., Haritashya, U. K., Kargel, J. S., and Karki, A.: Transition of a small Himalayan glacier lake outburst flood to a  
725 giant transborder flood and debris flow, *Sci Rep*, 12, 12421, 10.1038/s41598-022-16337-6, 2022.
- 726 Sattar, A., Goswami, A., Kulkarni, A. V., Emmer, A., Haritashya, U. K., Allen, S., Frey, H., and Huggel, C.: Future  
727 glacial lake outburst flood (GLOF) hazard of the South Lhonak Lake, Sikkim Himalaya, *Geomorphology*, 388,  
728 107783, <https://doi.org/10.1016/j.geomorph.2021.107783>, 2021.
- 729 Sattar, A., Cook, K. L., Rai, S. K., Berthier, E., Allen, S., Rinzin, S., de Vries, M. V. W., Haeberli, W., Kushwaha, P.,  
730 Shugar, D. H., Emmer, A., Haritashya, U. K., Frey, H., Rao, P., Gurudin, K. S. K., Rai, P., Rajak, R., Hossain, F.,  
731 Huggel, C., Mergili, M., Azam, M. F., Gascoïn, S., Carrivick, J. L., Bell, L. E., Ranjan, R. K., Rashid, I., Kulkarni,  
732 A. V., Petley, D., Schwanghart, W., Watson, C. S., Islam, N., Gupta, M. D., Lane, S. N., and Bhat, S. Y.: The Sikkim  
733 flood of October 2023: Drivers, causes, and impacts of a multihazard cascade, *Science*, 387, eads2659,  
734 10.1126/science.ads2659, 2025.
- 735 Sharma, S., Hamal, K., Khadka, N., and Joshi, B. B.: Dominant pattern of year-to-year variability of summer  
736 precipitation in Nepal during 1987–2015, *Theoretical and Applied Climatology*, 142, 1071-1084, 10.1007/s00704-  
737 020-03359-1, 2020.
- 738 Singh, A., Shrestha, D., Ghimire, K., Mishra, S., Rana, D., and Acharya, S.: Assessing machine learning models to  
739 generate permafrost distribution map in Solukhumbu, Nepal, *Geodesy and Geodynamics*, 16, 275-287,  
740 <https://doi.org/10.1016/j.geog.2024.08.003>, 2025.
- 741 Tai, Y.-C., Noelle, S., Gray, J., and Hutter, K. J. o. C. P.: Shock-capturing and front-tracking methods for granular  
742 avalanches, *Journal of Computational Physics*, 175, 269-301, <https://doi.org/10.1006/jcph.2001.6946>, 2002.
- 743 Thakuri, S., Salerno, F., Smiraglia, C., Bolch, T., D'Agata, C., Viviano, G., and Tartari, G.: Tracing glacier changes since  
744 the 1960s on the south slope of Mt. Everest (central Southern Himalaya) using optical satellite imagery, *The*  
745 *Cryosphere*, 8, 1297-1315, 2014.
- 746 Veh, G., Korup, O., and Walz, A.: Hazard from Himalayan glacier lake outburst floods, *Proc Natl Acad Sci U S A*, 117,  
747 907-912, 10.1073/pnas.1914898117, 2020.
- 748 Veh, G., Wang, B. G., Zirzow, A., Schmidt, C., Lützwow, N., Steppat, F., Zhang, G., Vogel, K., Geertsema, M., Clague, J.  
749 J., and Korup, O.: Progressively smaller glacier lake outburst floods despite worldwide growth in lake area, *Nature*  
750 *Water*, 3, 271-283, <https://doi.org/10.1038/s44221-025-00388-w>, 2025.
- 751 Vuichard, D. and Zimmermann, M.: The 1985 catastrophic drainage of a moraine-dammed lake, Khumbu Himal, Nepal:  
752 cause and consequences, *Mountain Research and Development*, 91-110, 1987.
- 753 Wang, X., Liu, S., Ding, Y., Guo, W., Jiang, Z., Lin, J., and Han, Y.: An approach for estimating the breach probabilities  
754 of moraine-dammed lakes in the Chinese Himalayas using remote-sensing data, *Natural Hazards and Earth System*  
755 *Sciences*, 12, 3109-3122, 2012.
- 756 Wang, X., Zhang, G., Veh, G., Sattar, A., Wang, W., Allen, S. K., Bolch, T., Peng, M., and Xu, F.: Reconstructing glacial  
757 lake outburst floods in the Poiqu River basin, central Himalaya, *Geomorphology*, 109063,  
758 <https://doi.org/10.1016/j.geomorph.2024.109063>, 2024.
- 759 Wang, X., Guo, X., Yang, C., Liu, Q., Wei, J., Zhang, Y., Liu, S., Zhang, Y., Jiang, Z., and Tang, Z.: Glacial lake  
760 inventory of high-mountain Asia in 1990 and 2018 derived from Landsat images, *Earth System Science Data*, 12,  
761 2169-2182, <https://doi.org/10.5194/essd-12-2169-2020>, 2020.
- 762 Wang, X., Chen, W., Zhang, G., Emmer, A., Frey, H., Taylor, C., Huggel, C., Sattar, A., Zheng, G., Rashid, I., Carrivick,  
763 J. L., Veh, G., Allen, S., Steiner, J., Quincey, D., and Mergili, M.: Mitigating future glacial lake outburst floods in  
764 the Himalaya, *Science Bulletin*, 71, 159-171, <https://doi.org/10.1016/j.scib.2025.11.024>, 2026.
- 765 Watson, C. S., Kargel, J. S., Shugar, D. H., Haritashya, U. K., Schiassi, E., and Furfaro, R.: Mass loss from calving in  
766 Himalayan proglacial lakes, *Frontiers in Earth Science*, 7, 2020.
- 767 Westoby, M. J., Glasser, N. F., Hambrey, M. J., Brasington, J., Reynolds, J. M., and Hassan, M. A. A. M.: Reconstructing  
768 historic Glacial Lake Outburst Floods through numerical modelling and geomorphological assessment: Extreme  
769 events in the Himalaya, 39, 1675-1692, <https://doi.org/10.1002/esp.3617>, 2014.



- 770 Worni, R., Stoffel, M., Huggel, C., Volz, C., Casteller, A., and Luckman, B.: Analysis and dynamic modeling of a  
771 moraine failure and glacier lake outburst flood at Ventisquero Negro, Patagonian Andes (Argentina), *Journal of*  
772 *Hydrology*, 444-445, 134-145, <https://doi.org/10.1016/j.jhydrol.2012.04.013>, 2012.
- 773 Zhang, G., Bolch, T., Yao, T., Rounce, D. R., Chen, W., Veh, G., King, O., Allen, S. K., Wang, M., and Wang, W.:  
774 Underestimated mass loss from lake-terminating glaciers in the greater Himalaya, *Nature Geoscience*, 1-6,  
775 <https://doi.org/10.1038/s41561-023-01150-1>, 2023a.
- 776 Zhang, T., Wang, W., and An, B.: A conceptual model for glacial lake bathymetric distribution, *The Cryosphere*, 17,  
777 5137-5154, <https://doi.org/10.5194/tc-17-5137-2023>, 2023b.
- 778 Zhang, T., Wang, W., and An, B.: A massive lateral moraine collapse triggered the 2023 South Lhonak Lake outburst  
779 flood, Sikkim Himalayas, *Landslides*, 22, 299-311, [10.1007/s10346-024-02358-x](https://doi.org/10.1007/s10346-024-02358-x), 2025.
- 780 Zhang, T., Wang, W., An, B., and Wei, L.: Enhanced glacial lake activity threatens numerous communities and  
781 infrastructure in the Third Pole, *Nat Commun*, 14, 8250, [10.1038/s41467-023-44123-z](https://doi.org/10.1038/s41467-023-44123-z), 2023c.
- 782 Zhang, T., Wang, W., Gao, T., An, B., and Yao, T.: An integrative method for identifying potentially dangerous glacial  
783 lakes in the Himalayas, *Sci Total Environ*, 806, 150442, [10.1016/j.scitotenv.2021.150442](https://doi.org/10.1016/j.scitotenv.2021.150442), 2022.
- 784 Zheng, G., Mergili, M., Emmer, A., Allen, S., Bao, A., Guo, H., and Stoffel, M.: The 2020 glacial lake outburst flood at  
785 Jinwuco, Tibet: causes, impacts, and implications for hazard and risk assessment, *The Cryosphere*, 15, 3159-3180,  
786 [10.5194/tc-15-3159-2021](https://doi.org/10.5194/tc-15-3159-2021), 2021a.
- 787 Zheng, G., Allen, S. K., Bao, A., Ballesteros-Cánovas, J. A., Huss, M., Zhang, G., Li, J., Yuan, Y., Jiang, L., and Yu, T.:  
788 Increasing risk of glacial lake outburst floods from future Third Pole deglaciation, *Nature Climate Change*, 11, 411-  
789 417, <https://doi.org/10.1038/s41558-021-01028-3>, 2021b.
- 790
- 791